Effect of Geological Heterogeneities on Reservoir Storage Capacity and migration of CO_2 Plume in a Deep Saline Fractured Carbonate Aquifer

M. Adeel Sohal*, [a], Yann Le Gallo [b], Pascal Audigane [c], J.Carlos de Dios [d], and Sean P. Rigby [a]

[a] Department of Chemical and Environmental, Engineering, University of Nottingham, United Kingdom.

[b] Geogreen, 2 rue des Martinets, 92569 Rueil Malmaison, France

[c] Bureau de Recherches Géologiques et Minières (BRGM), France

[d] Fundación Ciudad de la Energía, Avenida del Presidente Rodríguez Zapatero, 24492 Cubillos del Sil, Spain.

Abstract

In a reservoir characterization study of the Hontomín deep saline aquifer, the impact of geological heterogeneities on reservoir storage capacity and the migration of the CO_2 plume is explored. This work presents, for the first time, very long-term (up to 200 years) simulations of CO_2 injection into the naturally fractured Sopeña Formation, of the lower Jurassic age, at Hontomín. CO_2 injection was simulated as a dual permeability case with Eclipse compositional software. The matrix permeability of the carbonate reservoir is quite low (0.5 mD) and thus fluid flow through the fractures dominates. The reservoir is dissected by eight normal faults which limited its south-east extension and divided it into several segments. The effect of geological heterogeneities was tested through scenario-based modeling and variation of parameters characterizing heterogeneity within realistic limits based on other similar formations. This modeling approach worked well in Hontomín where the database is completely scarce. The plume migration, the reservoir storage capacity, and pressure, were each influenced in diverse ways by incorporating particular types of heterogeneities. The effect of matrix heterogeneities on reservoir storage capacity was substantial (by factors up to ~2.8×), compared to the plume migration. As the reservoir matrix permeability heterogeneity increased, the reservoir storage capacity markedly decreased, whilst an increase in porosity heterogeneity significantly increased it. The vertical gas migration in the homogeneous base case was relatively larger compared to the heterogeneous cases, and gas accumulated underneath the caprock via hydrodynamic trapping. It was also observed that, in heterogeneous cases, gas saturation in rock layers from top to bottom was relatively high compared to the base case, for which most of the gas was stored in the topmost layer. In contrast, the impact on storage capacity and plume movement of matrix vertical to horizontal permeability ratio in the fractured carbonate reservoir was small. The impact of the transmissibility of faults on reservoir pressure was only observed when the CO_2 plume reached their vicinity.

Keywords: CO_2 injection, Storage capacity, Geological heterogeneities, Injection pressure, limestone, Scenario-based modeling.

Contents

1 Introduction

Greenhouse gas emissions to the atmosphere can be mitigated by capturing and storing the carbon dioxide in subsurface geological formations, in order to stabilize its atmospheric concentration. Typically, CO_2 is injected in a supercritical ($scCO_2$) state and the minimum depth required to store it in this phase is approximately 800 m [1]. Although it is stored as $scCO_2$, it moves upward due to buoyancy (density difference between formation brine and supercritical phase) as described in the literature [2-4]. During its upward and lateral movement in a reservoir, CO_2 is mainly trapped in three different ways, in particular as a result of hydrodynamic trapping, solubility trapping, and mineral trapping because of stratigraphic and structural heterogeneities [5-18]. Different types of storage sites are available to store CO_2, namely coal beds, saline aquifers, depleted hydrocarbon reservoirs, and geochemical trapping in basalts. Saline aquifers have the largest storage capacity among the listed storage sites [19]. The main concern of CO_2 sequestration in saline aquifers is to minimize the risk of leakage at a maximum injection rate/volume. To determine the characteristic extent of the plume flow, the residence time of CO_2 volume, and reservoir storage capacity demands a detailed investigation of the subsurface reservoir. This might be available when CO_2 is stored in depleted oil reservoirs but it seldomly exists in saline aquifer cases. Therefore, scenario-based modeling is the best substitute during the initial assessment of an aquifer storage site when the database is scarce, as is often the case when CO_2 is to be stored in relatively unexplored saline aquifers. In that situation a deterministic field-scale reservoir model cannot be very accurate with respect to geological heterogeneities and fluid flow due to the uncertainties associated with the initial input parameters. Thus, scenario-based models taking expected site-specific geological heterogeneities into account are useful as part of the reservoir characterization and for planning the suitable injection and monitoring strategies. The motivation behind this work is to find the answer to the following questions in the simulation study.

- o   How geological heterogeneities affect the reservoir storage capacity?
- o   How sensitive is the plume migration to geological heterogeneities?

The impact of different types of geological heterogeneities on the migration of the CO_2 plume and reservoir storage capacity has mostly been investigated through conceptual reservoir models via parametric studies. The coefficient of variation (CV) of heterogeneities in those simulation models is always less than one [20]. The CV is a statistical measure of the dispersion of data points in a data series around the mean. It represents the ratio of the standard deviation to the mean, and it is a useful statistic for comparing the degree of variation from one data series to another, even if the means are drastically different from one another. The aforementioned models do not exhibit the level of heterogeneities that could be expected in a real field case. Therefore, in this simulation study of the Hontomín deep saline aquifer, the coefficient of variation was gradually increased to greater than one. The Hontomín site is an onshore deep saline aquifer located close to Burgos in the north of Spain and is operated by Fundación Ciudad de la Energía (CIUDEN, Cubillos del Sil, Spain). It was recognized by the European Parliament [21] as a key test facility for Carbon Capture and Storage (CCS) technology development. The $scCO_2$ is being stored in a naturally fractured limestone and dolomite reservoir of lower Jurassic age [22]. The geological model of the site was built by Geogreen and updated by the integration of the latest data, such as the image log interpretations from newly-drilled injection and observation wells [23].

The focus of this article is on the effect of matrix heterogeneity in a fractured system. This is because the interaction between the reservoir storage capacity and the extent of plume migration in a tight reservoir depends upon the matrix heterogeneity rather than the fractures, which act as conduits for fluid flow. Therefore, investigation of the fracture density and distribution was not part of this study, although the flow through the fractures dominates. One

particular area of interest was whether matrix heterogeneity accentuates or mitigates bypassing of the matrix by the plume flow in fractures for a tight reservoir. The plume migration (spread) depends on reservoir storage capacity, and, therefore, it was not possible to ignore one and calculate the other. In the work described below, the reservoir pressure is plotted against the injected cumulative mass of CO_2 and time to compare the reservoir storage capacity at the same pressure in different heterogeneous cases.

In this simulation study, the effect of heterogeneities on the migration of the CO_2 plume and reservoir storage capacity was explored with Eclipse (E300) software using the dual permeability option. There is no time-lapse seismic dataset available in the Hontomín case to validate the CO_2 plume movement in different layers of the Sopeña Formation against the simulation model. Predicting the CO_2 flow behavior in naturally fractured carbonate reservoirs is quite challenging compared to other lithologies especially when the database is completely scarce. Therefore, scenario-based modeling can reveal the best field development strategy for long-term CO_2 storage as well as the potential challenges that could be envisaged in different possible geological settings. A gradual increase in CV value to greater than one provided an insight into the effect of the level of heterogeneity variation on plume migration and storage capacity. Moreover, the influence of the variation of individual matrix and fracture permeabilities at the same rate of migration and storage of CO_2 were explored and compared.

1.1   Geological Model Description

The geological model of the Hontomín site is a structural dome and includes under-burden, reservoir, seal, and overburden. The vertical cross-section of the whole geological complex is shown in Figure 1, which was constructed through the analysis and integration of borehole images, well logs, and well test data [23]. The overburden comprises of the Dogger, Purbeck, and Weald Formations of late Jurassic to lower Cretaceous age and is placed unconformably on top of the middle Jurassic marine rocks [22]. The formations are mainly composed of clays, sandstone, and carbonate rocks, and the depth of these formations changes along with the structure. The caprock is mainly composed of highly carbonated marls (close to 50% of its composition) and consists of the Pozazal and Marly Lias Formations of middle Jurassic age which are approximately 163 m thick at the well location. The lower Jurassic Sopeña formation is the reservoir and it is composed of fractured limestone in the upper part and dolomites in the lower part. The reservoir limestone is located at a depth of 1435 m in the injection well (HI) and is 79 m thick, whereas the dolomite was found at a depth of 1514 m in HI and is 41 m thick. Therefore, the total reservoir thickness is 120 m at the injection well location. The reservoir has an increasing dip towards the north and north-east from the injection well, with its apex around the H2 legacy well [23]. The reservoir was modeled with 39 layers, and the thicknesses of layers vary from 1 to 10 m. The matrix permeability of the reservoir is approximately a half milli-Darcy in the geological model and the porosity varies from 3 to 13 %. The Keuper formation of the Triassic age is the under-seal, located at a depth of 1555 m in the HI well, and is mainly composed of anhydrite. A total of five geological facies (limestone, dolomite, marls, shale, and anhydrite) was included in the geological model. The permeability and porosity of different facies were assumed to be constant in the model and available from the hydraulic characterization tests [23, 24]. The permeability of marls, shale, and anhydrite is almost zero, whereas limestone and dolomite matrix permeabilities are in the range of ~0.5 mD [23]. These values were determined during the hydraulic characterization campaigns conducted on-site [24].

There are eight normal faults inferred at the top of the reservoir from the 3-D seismic interpretations, and are assumed to be vertical within the reservoir. Two main faults cross the storage complex from the reservoir to the overburden, which limits the south-eastward extension of the reservoir. These are the Ubierna fault, located at the southern part, and the East fault located at the eastern part of the Hontomín site, as shown in Figure 2. The boundary faults (Ubierna & East faults) are supposed to be sealing faults and the transmissivity of all other faults in the

geological model is unknown. There are four legacy wells; H1, H2, H3, and H4, located in the study area; these wells were commonly used to confirm the structure, geometry, and properties of the whole geological complex. However, the main source to gather data for the geological model was the newly drilled observation (HA) and injection (HI) wells. Petrophysical properties are known only around the well drainage area. However, their properties are uncertain in the rest of the reservoir and could be varied to match the observed data in the history matching process.
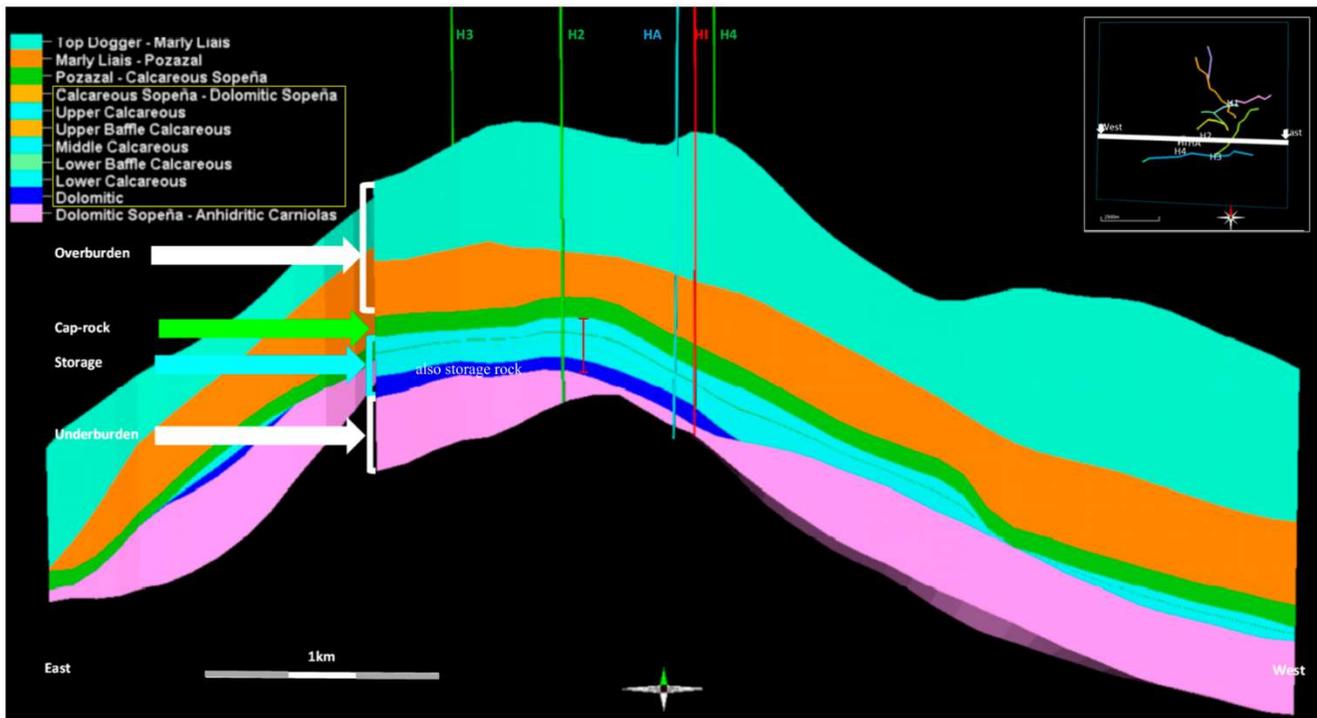
Figure 1. Vertical cross-section of the geological model of the Hontomín storage complex; The HA and HI newly-drilled wells are the observation & injection wells, respectively, while well H1 to H4 are legacy wells [23]. The legacy wells were used to confirm the geological sections & reservoir geometry.
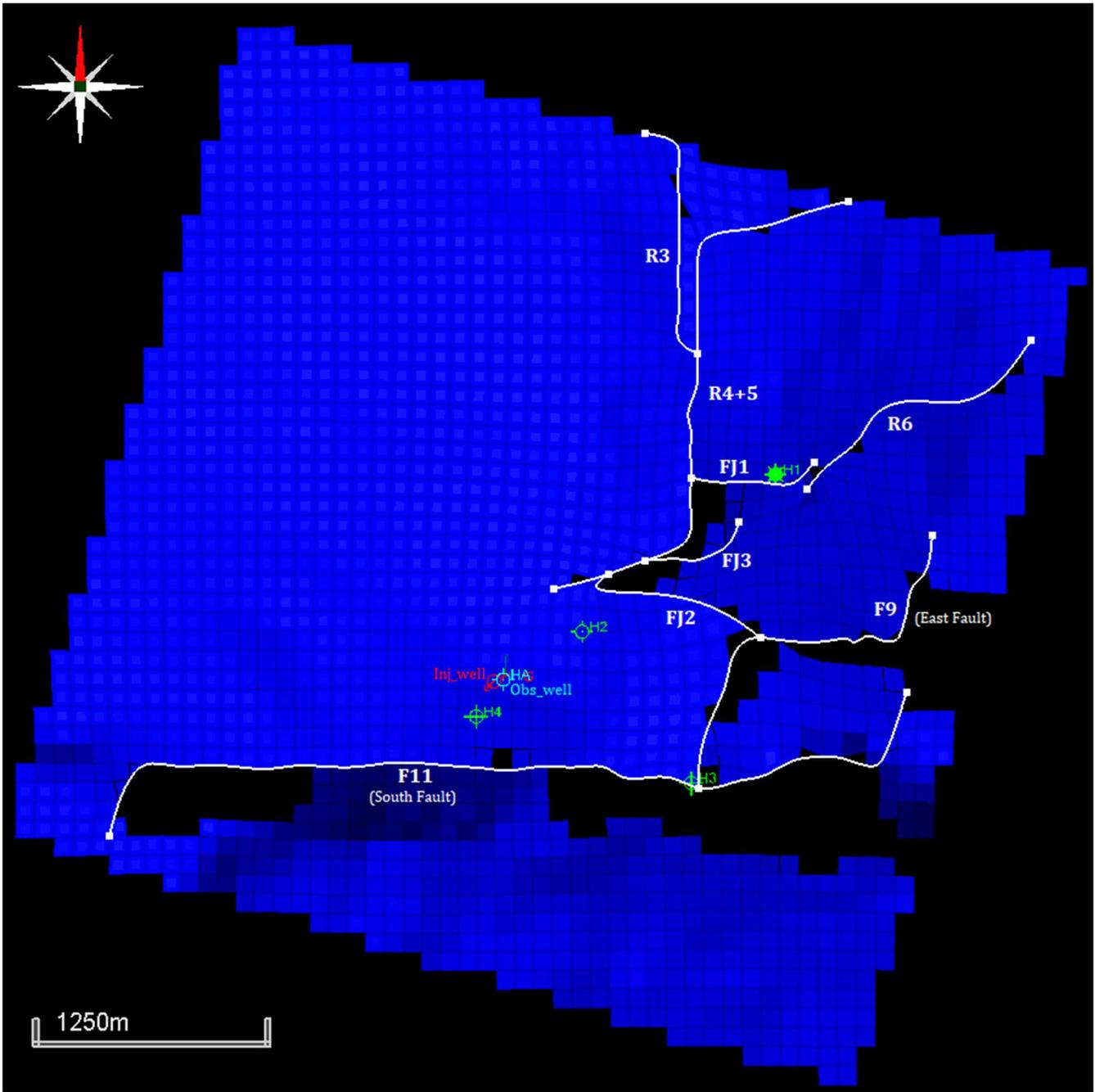
Figure 2. Location of wells and the extensions of all the eight faults within the Hontomín geological model in Petrel. F11 (South Fault) is located in the south, while the F9 (East Fault) is located on the east side and controls the structural extension of the reservoir in the south-east direction.

2   Modeling Approach

In this study, the effects of geological heterogeneities on reservoir storage capacity and the migration of the CO_2 plume were investigated during long term injection in the Sopeña Formation. Since the Sopeña Formation is highly fractured, it was simulated by using the dual permeability option within E300. The dual-permeability model assumes that the matrix is permeable and allows the flow between matrix blocks, in addition to matrix-fracture and, a fracture-fracture flow which is observed in a dual-porosity model [25, 26]. The dual-porosity model consists of two regions with distinct porosities and permeabilities, representing the matrix and fractures within the formation. The matrix constitutes the region with negligible flow capacity but significant pore volume that is providing the primary porosity to the reservoir system. The fracture system provides the path for fluid flow from the formation to the well and does not contribute to storage. Several studies pointed out that the dual-porosity model may not be appropriate for interpreting the well tests data from all fractured reservoirs [27]. The Hontomín homogeneous model was initially history matched with water-alternating-gas (WAG) well test data and then used to simulate long-term CO_2 injection. During the long-term CO_2 injection, the effect of geological heterogeneities, vertical to horizontal matrix permeability ratio (k_v/k_h), and fault transmissibilities were explored. The dimensions of the Sopeña formation in the Hontomín geological model are 5.7 km by 5.6 km with a thickness of 120 m. The horizontal matrix permeability (k_h) is 0.5 mD, the vertical matrix permeability (k_v) was set to 0.05 mD, and the porosity varies from 3 to 13 % in the calibrated homogeneous model. The model was considered initially in hydrostatic equilibrium, with an initial reservoir pressure of 141 bar at a True Vertical Depth (TVD) of 1459 m. The initial water saturation (S_w) was 100% and the salinity of the formation water was 40,000 ppm. There was no dissolved gas in the aqueous phase at the beginning of the simulation. The Hontomín geological model was uniformly gridded in the horizontal direction with 57 cells in the X-direction, 56 in the Y-direction and 658 cells in the Z-direction with different thickness. The reservoir model details are summarized in Table 1.

Table 1. The details of the homogeneous simulation model of Hontomín deep saline aquifer.

Parameters	Values	Units
Total grid cells	2,103,528	
Reservoir length	5.7	km
Reservoir width	5.6	km
Reservoir thickness	0.5	m
Matrix horizontal permeability	202	mD
Matrix vertical permeability	0.05	mD
Matrix porosity	3-13	%
Fracture permeability in x-direction	240	mD
Fracture permeability in y-direction	360	mD
Fracture permeability in z-direction	360	mD

Fracture porosity	0.01	
Net to gross ratio	1	
Sigma	1	
Reservoir depth (TVD)	1459	m
Reservoir pressure	141	Bar
Reservoir temperature	42	°C
Initial water saturation (Swi)	1	%
Residual water saturation	10	%
Water endpoint relperm	1	
Residual gas saturation	0.05	%
Gas end point relperm	0.9	
Pore brine salinity	40,000	ppm
Components	H_2O, CO_2	
Pore brine density	1.002	g/cm^3
FVF	1.01	Rm^3/Sm^3
Pore brine viscosity	0.66	cP

2.1   Relative Permeability and Capillary Pressure Data

In the literature, different CO_2 brine relative permeability curves for carbonate rocks have been proposed, but the following set of drainage relative permeability curves, measured in the Wabamun Limestone Formation [28] were initially used in this simulation study. However, the relative permeabilities for matrix and fractures were further adjusted with the help of Corey's model [29] for gas water system as given in Eqs. (1) and (2):

$$k_{rg} = k_{rg(wir)} \left[\frac{S_g - S_{gr}}{1 - S_{gr} - S_{wir}} \right]^{ng} \quad (1)$$

$$k_{rw} = k_{rw(gr)} \left[\frac{S_w - S_{wir}}{1 - S_{gr} - S_{wir}} \right]^{nw} \quad (2)$$

where S_{wir} is the irreducible water saturation, S_{gr} is residual CO_2 saturation, and Nw and Ng are Corey's functions for water and CO_2 respectively. The values of parameters to generate the Wabamun and the current model drainage relative permeability curves are given in Table 2. In the initial model validation process, the same relative permeability curves were used to model CO_2 displacing water and water displacing CO_2 (i.e., no hysteresis in relative permeability). The impact of relative permeability hysteresis on geological CO_2 storage can be found elsewhere [30]. The final relative permeability curves for matrix and fractures are shown in Figure 3.

Table 2. The details of the parameters which were used to generate the drainage relative permeability curves for Wabamun and the Hontomín Limestone.

Parameters	Wabamun (drainage)	Hontomín
S_{gr}	0.005	0.05
Ng	5.60	2
$Krg@S_{wir}$	0.5289	0.9
S_{wc}/S_{wir}	0.5950	0.1
Nw	1.40	1
$Krw@S_{gr}$	0.970	0.945
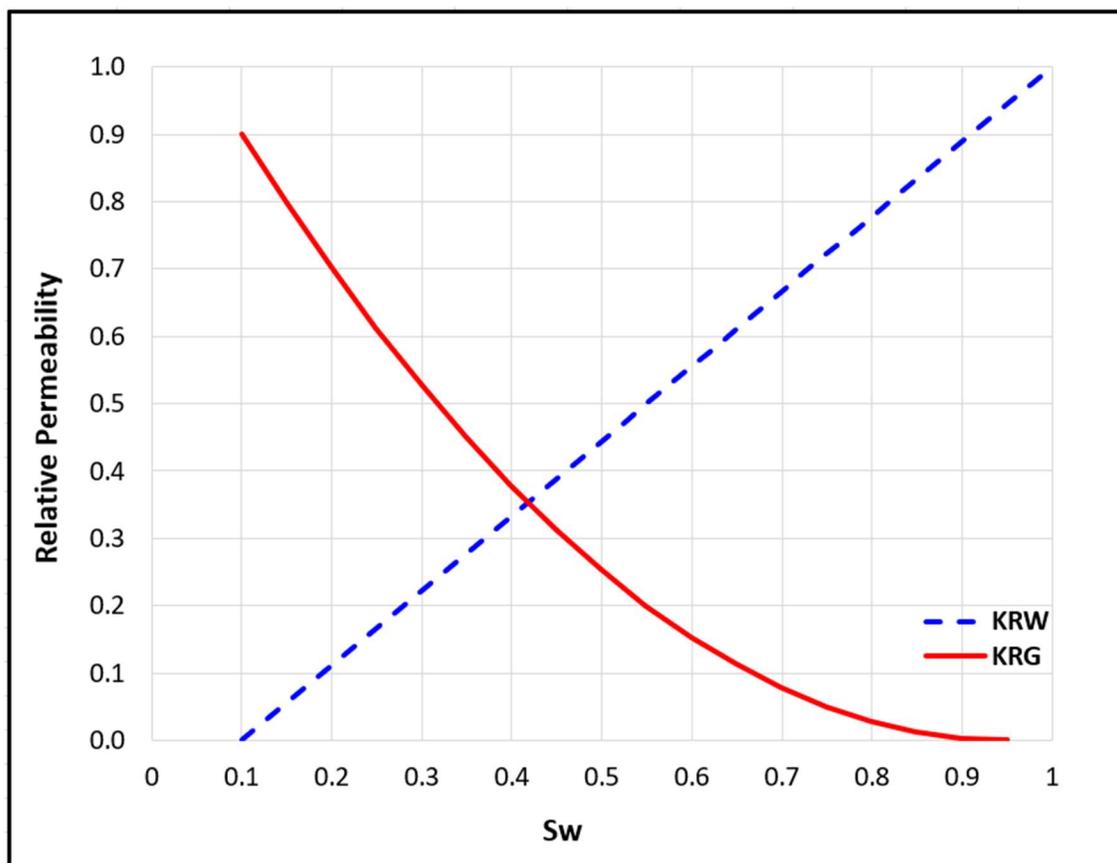
Figure 3. The relative permeability curves for matrix and fractures that were used in the history matching process.

It was found, from the petrophysical lab results, that 38%–78% of the pore throats within the Sopeña Formation are in the micropore scale (< 2 nm) range according to the International Union of Pure and Applied Chemistry (IUPAC) classification of pore size. Therefore, the pore entry pressure (capillary pressure) for the majority of the rock pores is greater than the CO_2 injection pressure. Consequently, CO_2 will not invade a significant part of the reservoir rock during the injection period and principally migrate through the fractures. The capillary pressure curve was calculated by the Brooks and Corey model [30] in Petrel by using the input parameters given in Table 2 and depicted in Figure 4.
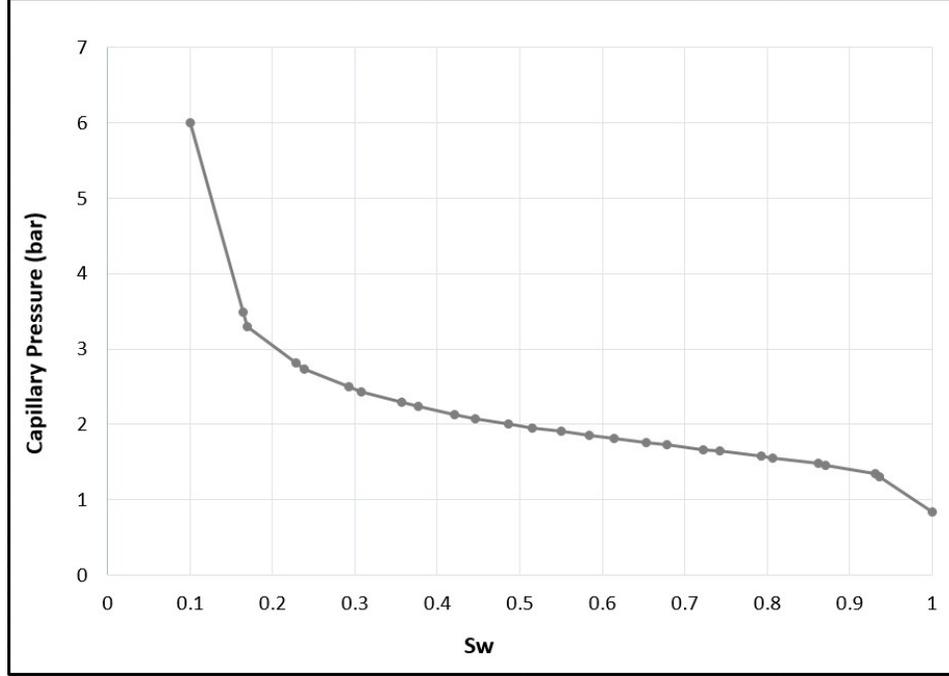
Figure 4. A capillary pressure curve that was used in the validated base case.

2.2 Fluid Properties

The Eclipse compositional (E300) software calculates the density of CO_2 by using a cubic equation of state which is accurately tuned to give the density of the compressed gas phase by following the method given in Spycher and Pruess [31]. A modified Peng Robinson equation of state is used, where the attraction parameter is made temperature-dependent. The gas viscosity is calculated from the method of Fenghour and Wakeham [32]. The mean pore brine density without any dissolved CO_2 was 1002 kg/m³, based on a salt mass fraction of 0.038. The viscosity of brine was calculated using the viscosity of water given in the International Association for the Properties of Water and Steam (IAPWS), 2008 [33] with the help of Eqs. 3 and 4 as described by Sharqawy et al. [34].

$$\mu_{sw} = \mu_{sw} \left(1 + AS + BS^2\right) \quad (3)$$

$$A = 1.541 + 1.998 \times 10^{-2}\, t - 9.52 \times 10^{-5}\, t^2$$
$$B = 7.974 - 7.561 \times 10^{-2}\, t + 4.724 \times 10^{-4}\, t^2$$

$$\mu_w = 4.2844 \times 10^{-5} + \left(0.157(t + 64.993)^2 - 91.296\right)^{-1} \quad (4)$$

The mutual solubility of CO_2 and H_2O in E300 is calculated to match the experimental data for typical CO_2 storage conditions for a temperature range between 12–250 ºC and pressure up to 600 bars. They were calculated following the procedure given by Spycher and Pruess [17, 31], based on fugacity equilibration between water and a CO_2 phase. Water fugacity was obtained by Henry's law, while CO_2 fugacity was calculated using a modified Redlich-Kwong equation of state.

3   History Matching and Model Calibration

Hontomín is a low permeability and a highly fractured carbonate reservoir. Therefore, it was simulated by a dual permeability option in E300. The dual permeability option in a reservoir simulator involves a highly interconnected set of fractures which are uniformly distributed throughout the reservoir. The simulator divides the whole reservoir into an equal number of matrix and fracture grid blocks, unlike a real reservoir system. This model of an idealized fracture system was initially introduced by Warren & Root [35] and has been commonly used since then. The Hontomín model was calibrated against the well test brine and WAG data, and constructed as a homogeneous model. The model validation process commenced with an assisted history matching method utilising a Petrel uncertainty and optimization workflow, and, later on, the best match was manually tuned. In the validation process, capillary pressure and local grid refinement (LGR) around the well were tuned otherwise it was not possible to get a good match to the observed data. In the history matching process, more than 850 realizations were simulated with a reasonable range of uncertain parameters. Initially, calculation of the fracture permeability and porosity for fractured carbonate reservoirs was achieved by employing the method given by Nelson [36]. However, due to the many unknown input parameters, each was then treated as a free-fitting parameter in the history matching process. Similarly, fluid compressibility and formation volume factor were calculated by the method described by Tarek Ahmed [37]. The impact of each uncertain reservoir parameter on the bottom-hole pressure was thoroughly investigated in the process of getting a good final match to the history data. The match of reservoir bottom-hole pressure achieved by the simulated data for all the well test campaigns is depicted in Figure 5.
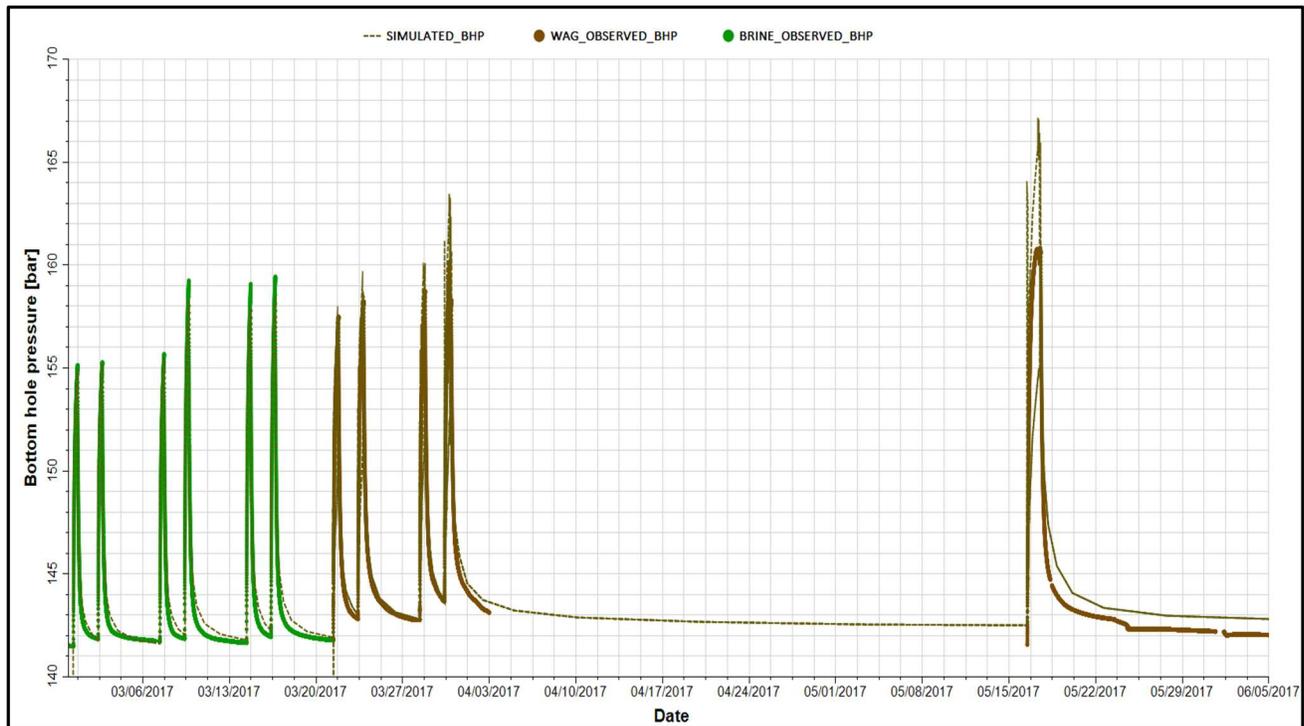
Figure 5. History matching of the simulated bottom-hole pressure for the Hontomín model with brine and WAG well test observed data respectively for 2017.

4   Results and Discussion

4.1   Simulation Results for Homogeneous Model

In the homogeneous Hontomín simulation model, the best match during the history matching process to the observed well test WAG data was achieved using a matrix permeability (k_m) of 3mD for limestone and dolomite facies and with k_m almost constant throughout the Sopeña reservoir. Therefore, all the layers of the Sopeña reservoir were equally likely for CO_2 migration. Fracture permeabilities within the Sopeña reservoir were set 1.5 times higher in the E—W direction compared to the N-S direction. It has been identified, by Le Gallo and de Dios [23] from the Tele-viewer log interpretation, that the number of fractures in the E-W direction (278) is greater than the number of fractures in the N-S direction (48). In the well test historical data, slugs of brine and CO_2 were injected into the Sopeña Formation, and the average injected volume of brine and gas in each slug was approximately 21 and 28333 sm^3 for brine and CO_2 respectively. Slugs of brine and CO_2 were continued for two days in WAG injection fashion and ceased for three days before the start of the next slug. The plot of water and CO_2 WAG-type slug injection pressure for the initial three years is shown in Figure 6 and a small-scale plot of the pressure versus injection rate for gas slugs is depicted in Figure 7 to show the slug injection pattern. The reservoir shut-in pressure rose from 14,300 to 14,900 kPa during the brine and gas slug injections over 30 years. However, the injection pressure rose to 16,300 kPa at the beginning (July 2017) and then gradually declined to 15,700 kPa until April 2019, and then, again, steadily increased to 15,900 kPa over the next 30 years injection time. This pressure behaviour observed shows the greater ease of the gas flow with time in a homogeneous reservoir, which could be associated with increasing gas relative permeability due to an increase in gas saturation. The historical data for the WAG process indicated it started with water injection possibly to make sure the gas would flow away from the well into the reservoir. The validated homogeneous simulation model was used as a reference case (denoted below as the 'base case'). against which all other simulated cases were compared to determine the impact of the changes in a sensitivity study.
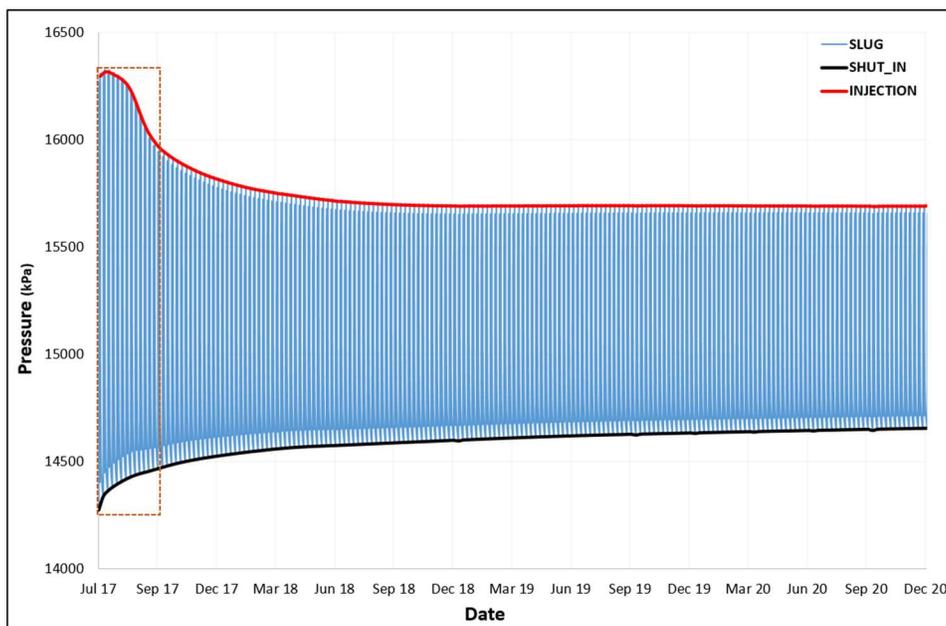
Figure 6. Build-up and shut-in reservoir pressures during water alternating gas slug injections in the homogeneous base case. The boxed part of the plot is shown on a smaller scale in figure 7.
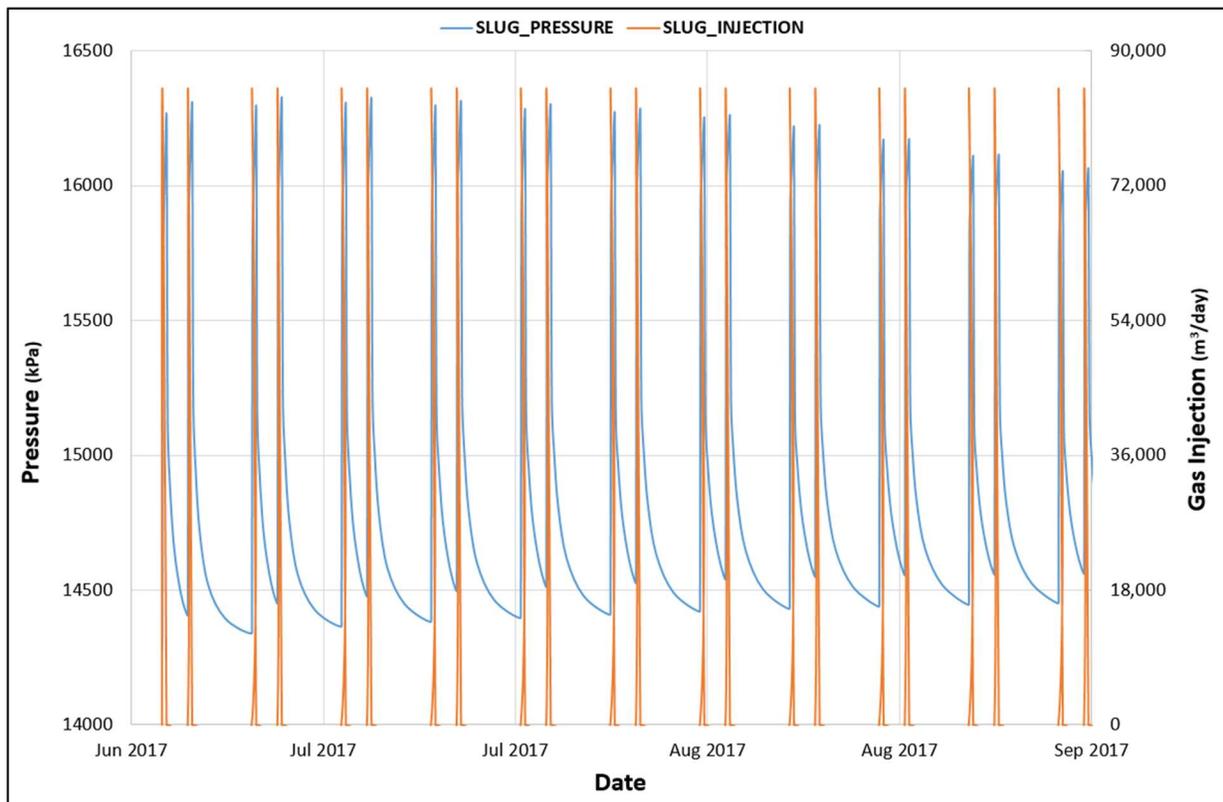
Figure 7. Small scale display of CO_2 slug injection rate and pressure during the WAG process in the homogeneous base case.

4.2 Simulation Results of Heterogeneous Models

Several heterogeneous models were simulated by altering the matrix permeability and porosity in order to investigate the impact of these changes on CO_2 plume migration, reservoir storage capacity, and pressure. The heterogeneous models were created using a sequential Gaussian simulation method [38] and ranked based on the coefficients of variation of the porosity and permeability. As mentioned above, the base model for these heterogeneous cases is the validated homogeneous model, known as the base case. It served as a reference against which to compare the changes resulting from the various heterogeneous models. There are six reservoir zones in the geological model and each reservoir zone has a different minimum, maximum, mean, and standard deviation value for matrix porosity and permeability. The permeability was log-normally distributed, while the porosity was normally distributed, amongst the various reservoir zones. In all the heterogeneous cases the mean values were close to the base case, but the standard deviation was different. The level of heterogeneity amongst the models was gradually enhanced by increasing the standard deviation of the given parameter, which meant the spread of the properties around the mean value increased. It is noted that, in Petrel, it is not possible to produce heterogeneous models with identical mean values by changing only the standard deviation, and minimum and maximum for the range of the properties. Therefore, the mean value of heterogeneous cases slightly varies from the base case, as well as from each other.

4.2.1 Heterogeneity Based on Permeability

A comparison of the matrix permeability for all the six zones of a typical heterogeneous case (base_13) with those of the homogeneous base case is given in Table 3 and displayed in Figure 8. The degree of heterogeneity is characterized by the coefficient of variation. Therefore, the degree of heterogeneity of geological models, based on the coefficient of variation for matrix permeability, relative to the base case is given in Table 4. The typical reservoir matrix permeability is 0.5mD, and, therefore, it has been varied in a range between 0.01 to <10mD to produce the heterogeneous cases. This variation is within the range of the permeability distribution which was observed in the Turonian – Campanian Kometan Formation [39], which is a similar tight limestone reservoir located in the north of Iraq. The heterogeneous cases thus produced are in a realistic range of permeability heterogeneity and tested to observe the minimum and maximum reservoir response which could be anticipated during and after the injection campaigns. It will be seen the heterogeneity affected the migration of CO_2 plume reservoir storage and pressure differently.

Table 3. The permeability distribution range, standard deviation, and coefficient of variation for each zone of the reservoir for the given two cases.

Cases	Reservoir Zones	k_{min}	k_{max}	k_{mean}	Stdv	CV
BASE CASE	Upper calcareous	0.0	3.0	2.9	0.4710	0.16
	Upper baffle calcareous	0.0	3.0	2.0	1.4171	0.71
	Middle calcareous	3.0	3.6	3.1	0.2548	0.08
	Lower baffle calcareous	3.0	3.6	3.3	0.2961	0.09
	Lower calcareous	3.0	3.6	3.0	0.1213	0.04
	Dolomitic	0.0	0.6	0.6	0.0622	0.10
BASE_13	Upper calcareous	0.04	9.96	2.4	2.0606	0.85
	Upper baffle calcareous	0.02	9.99	2.0	2.6706	1.34
	Middle calcareous	0.08	9.86	2.3	1.9921	0.89
	Lower baffle calcareous	0.20	9.22	2.0	1.4631	0.72
	Lower calcareous	0.9	9.97	3.0	2.4277	0.81
	Dolomitic	0.01	10.0	0.4	1.0018	2.45

Table 4. The coefficient of variation of matrix permeability for the set of simulated heterogeneous cases.

Cases	Base case	Base_1	Base_2	Base_3	Base_4	Base_5	Base_6	Base_7	Base_8
CV<1	0.46	0.77	0.81	0.85	0.88	0.91	0.94	0.97	0.99
Cases	Base_9	Base_10	Base_11	Base_12	Base_13	Base_14	Base_15	Base_16	Base_17
CV>1	1.02	1.04	1.07	1.09	1.11	1.19	1.26	1.32	1.38
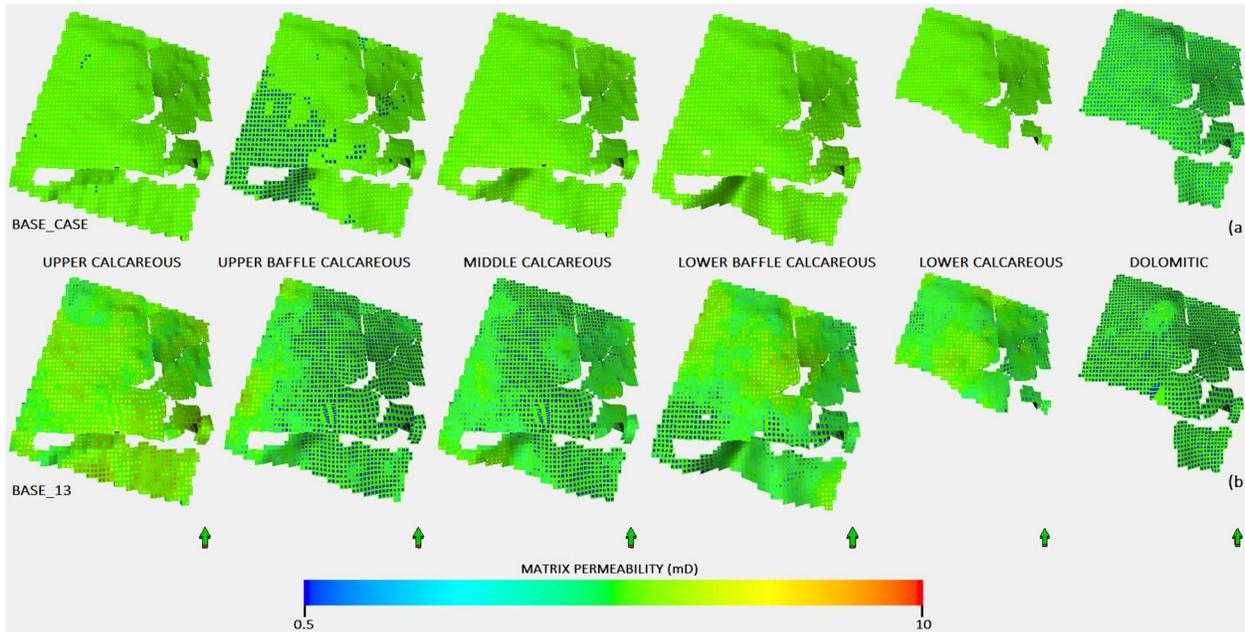
Figure 8. Comparison of matrix permeability distribution in X-direction for the homogeneous base case with that for the heterogeneous case (base_13).

4.2.1.1 *Reservoir Pressure and Heterogeneity*

It was observed that the reservoir shut-in pressure increased as the level of heterogeneity increased. However, the rise in pressure with respect to the homogeneous base-case was small at the given injection rate over 50 years. It can be seen in Figure 9 that the shut-in pressure continuously increased with time as long as gas was being injected. However, the pressure rise, in the beginning, was quite sharp but declined with time. The sharp pressure gradient, in the beginning, could be due to the slow mobility of CO_2 which was improved as the gas saturation increased with time. The mobility of the gas phase increased as its relative permeability increased which depended on gas saturation in the porous media. The pressure response depended on the matrix permeability distribution in each layer of a reservoir zone and it increased as the permeability heterogeneity increased. The build-up pressure trend in the cell containing the injection well is depicted in Figure 10 and it illustrates that the pressure is inversely related to the permeability distribution in the same grid cell. While the change in pressure response is relatively low in absolute terms in this dual permeability case because the permeability difference among the layers is small, nonetheless it still gives an insight into a pressure variation trend that may well be non-trivial in a single permeability case depending on permeability variation among the layers.
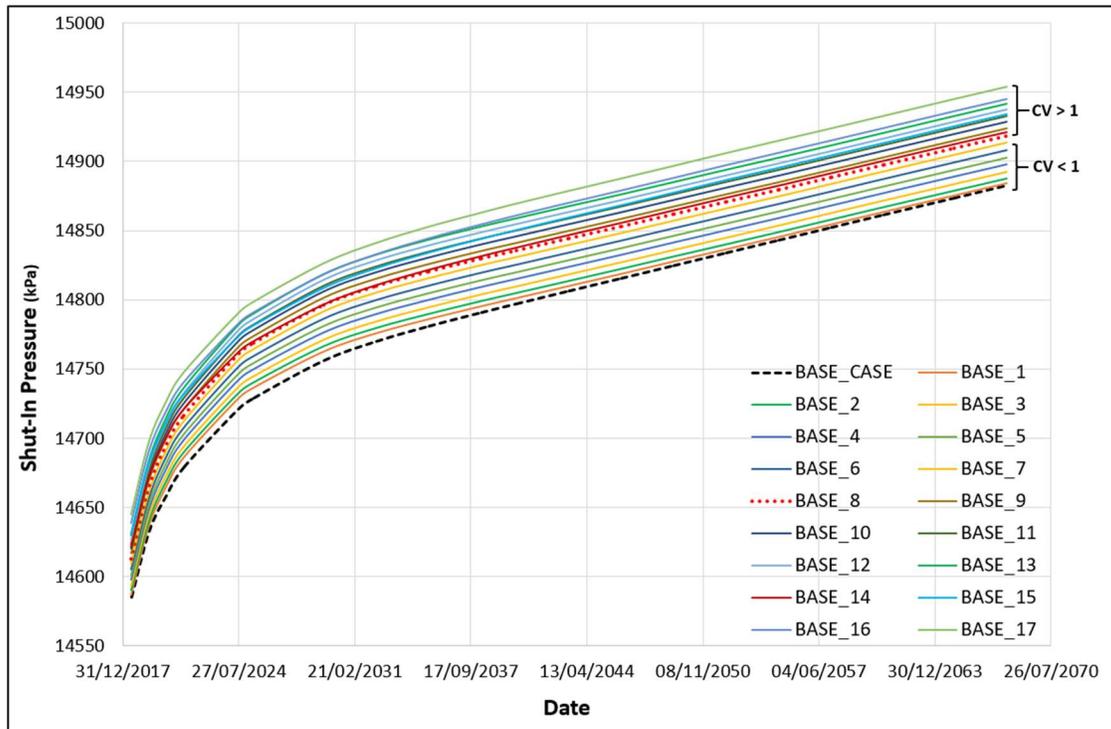
Figure 9. The variation of reservoir shut-in pressure, over 50 years of gas injection, with increased heterogeneity in matrix permeability in the horizontal direction.
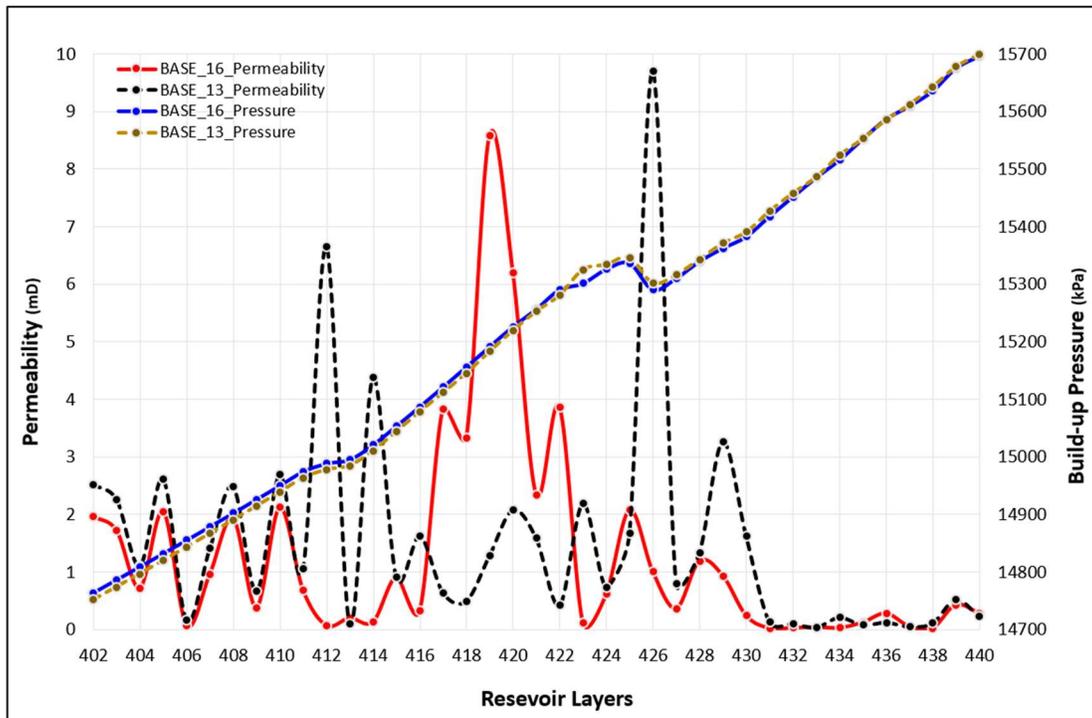
Figure 10. The relationship between permeability and pressure build-up for each layer of the reservoir as it was recorded in the grid cells that were penetrated by the injection well. The pressure build-up is inversely proportional to the matrix permeability in this case.

4.2.1.2   Reservoir Storage Capacity and Heterogeneity

The impact of geological heterogeneities on reservoir storage capacity was investigated by injecting CO_2 at a constant rate instead of constant pressure. Therefore, the reservoir storage capacity was derived from a change in reservoir pressure by injecting a similar volume of gas over the same period of time into different heterogeneous models. The reservoir shut-in pressure versus cumulative CO_2 injection for different simulated cases, as compared to the base case, is shown in Figure 11. It is obvious, from the comparison of these various cases with the base case, that, as the reservoir matrix permeability heterogeneity increased, the storage capacity markedly decreased. The comparison of base case with base_17 at reservoir shut-in pressure of 14,826 kPa showed that the reservoir storage capacity decreased approximately 2.8 times for this highly heterogeneous case. In the dual permeability simulated model of Hontomín, heterogeneity based on matrix permeability adversely affected the reservoir storage capacity. In carbonate reservoirs, an increase in permeability is associated with pore connectivity as observed by Ling et al. [40].
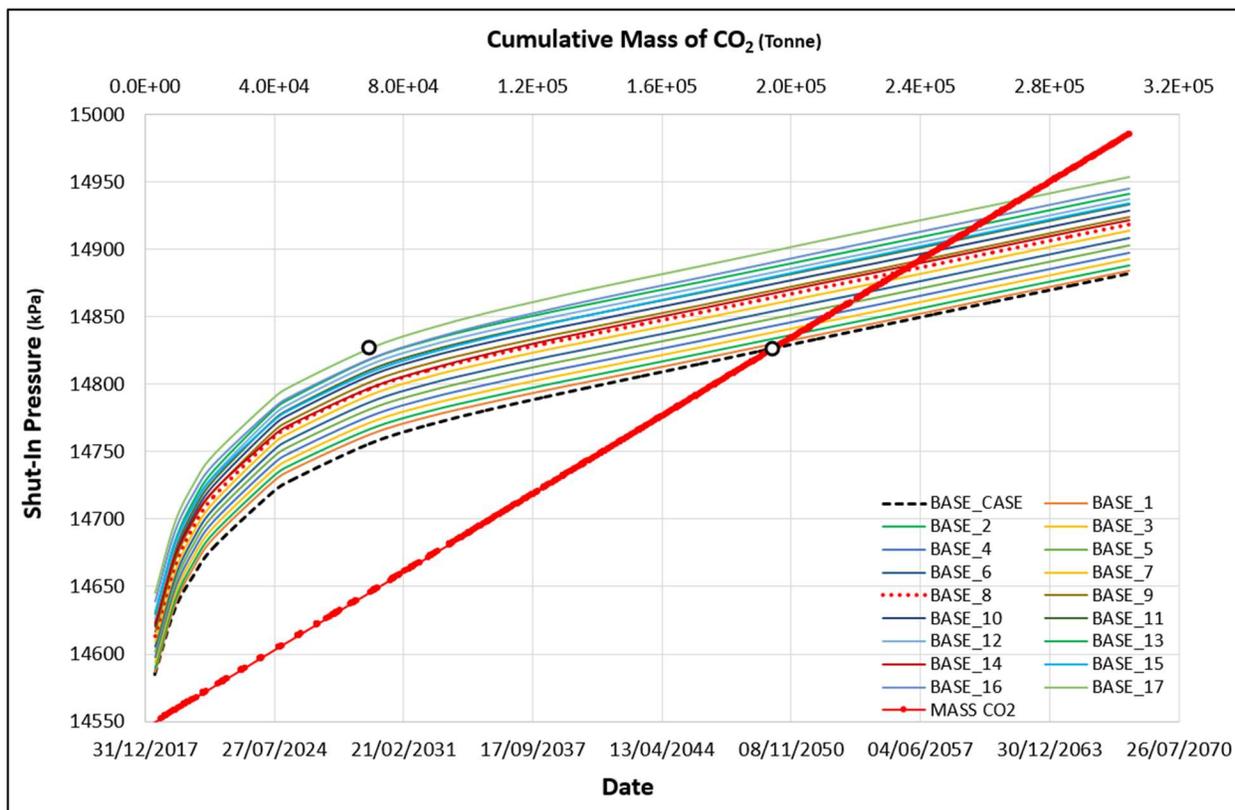
Figure 11. Reservoir shut-in pressure versus the cumulative injected mass of CO_2 for a similar time period. The heterogeneity of the simulated models based on the variation in matrix permeability.

4.2.1.3   Migration of CO_2 Plume and Heterogeneity

The CO_2 plume migration, in the horizontal and vertical directions away from the injection well, for base case and base_16, is portrayed in Figure 12. The spread of the CO_2 plume in the topmost zone of the reservoir slightly varied between these two cases although the heterogeneity difference based on matrix permeability was quite significant. This could be a consequence of dual permeability modelling in which flow took place between fracture

and matrix as well as between matrix and matrix. Therefore, the plume relatively migrated more in the south-west direction in base_16 compared to the base case. The vertical gas migration in a homogeneous case is relatively larger compared to the heterogeneous case and gas is accumulating underneath the caprock which is known as hydrodynamic trapping. For the heterogeneous case, gas saturation in rock layers from top to bottom is relatively high compared to the base case for which most of the gas is stored in the topmost layer. The horizontal plume migration among the layers also depends on the part of the reservoir perforated for the injection well for gas injection, which was the entire reservoir zone in this case. Thus, each zone of the reservoir in all heterogeneous cases was equally open for gas injection like the base case.
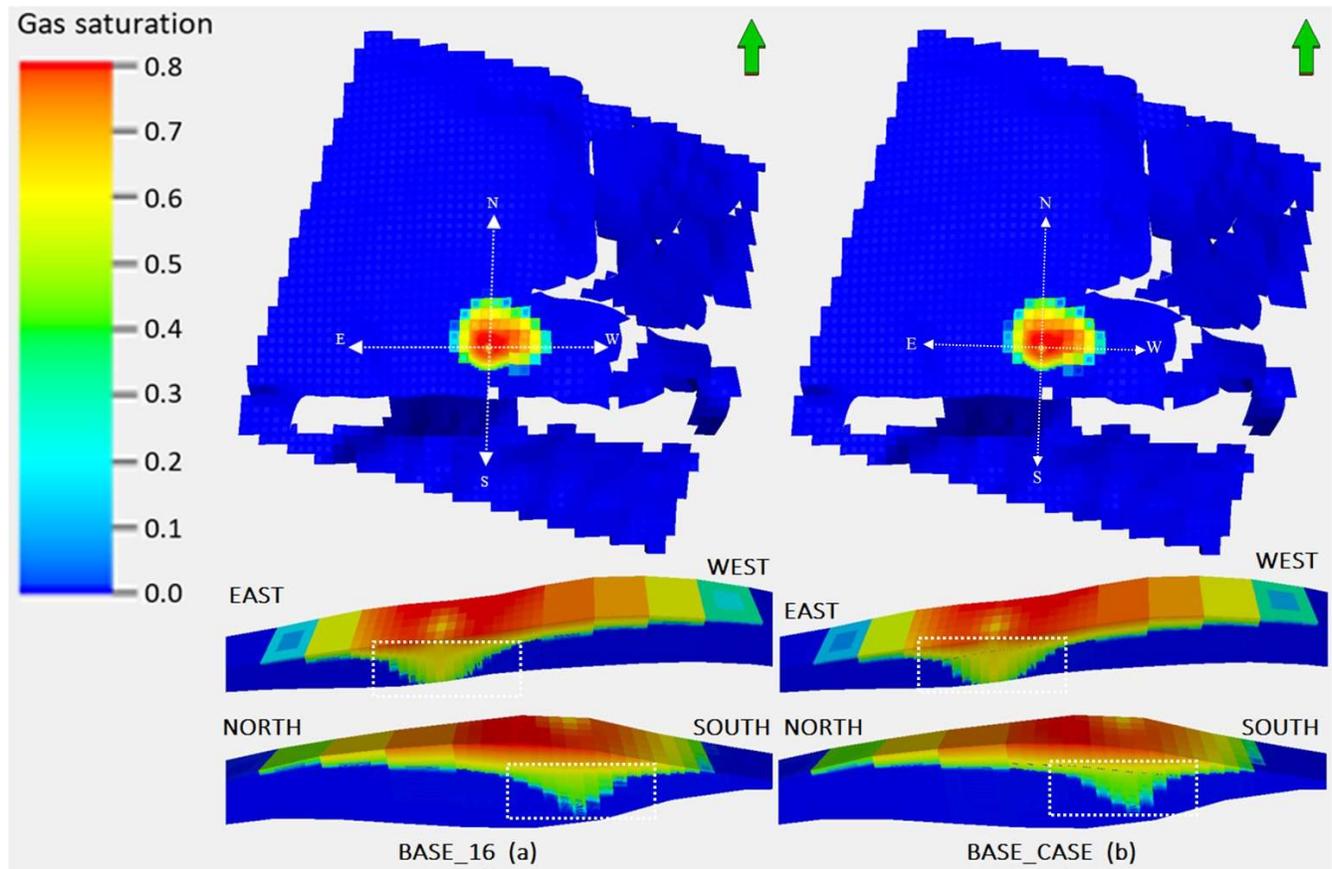
Figure 12. Part (a) shows the migration of CO_2 plume in base_16 and part (b) shows the migration of CO_2 plume in the homogeneous base case over 50 years of injection. The same volume of CO_2 was injected in both cases but the migration of plume was different in the heterogeneous case because of the variation in matrix permeability distribution.

4.2.2 Heterogeneity Based on Porosity

In most previous studies [41-46], the assigned porosity is taken as uniform since it is a common assumption that the heterogeneity for flow simulations may be manifested entirely in the hydraulic conductivity field, and that variations in porosity have negligible effects on fluid flow. However, we contend that it is also very important to characterize and incorporate heterogeneity of porosity in transport modelling, since it could induce irregular plume distributions, delay and spread solute breakthrough curves, and increase plume second moments as observed

previously [46-49]. Therefore, porosity heterogeneity must be incorporated into reactive transport simulations to more accurately evaluate CO_2–brine–rock interactions.

The degree of heterogeneity of geological models based upon matrix porosity relative to the base case is described by the coefficient of variation and values are given in Table 5. The method to produce the heterogeneous models based on porosity heterogeneity is similar to that used for permeability. The heterogeneity based on porosity affected the migration of the CO_2 plume and reservoir storage capacity differently compared to the heterogeneity based on matrix permeability.

Table 5. The coefficient of variation in matrix porosity for the set of simulated cases.

Cases	ϕ_{min}	ϕ_{max}	ϕ_{mean}	Stdv	CV
Base case	3%	13%	7%	0.0094	0.13
Base_72	1%	20%	9%	0.0481	0.51
Base_73	1%	20%	10%	0.00542	0.52
Base_74	1%	20%	9%	0.0497	0.55
Base_75	1%	20%	10%	0.0569	0.58

The plume migration away from the injection well was significantly different between the homogeneous base case and the heterogeneous case (base_72) as can be seen in Figure 13. An equal amount of CO_2 was injected in both cases over 50 years, and at a similar injection rate. The heterogeneous case base_72 increased the reservoir storage capacity by a factor of 1.5 times more than the base case at the shut-in pressure of 14,806 kPa as shown in Figure 14. It was found that plume spread is inversely related to available pore volume as arising from the variation in the heterogeneous porosity distribution. Reservoir shut-in pressure was 42.5 kPa higher in the base case compared to the heterogeneous case over 50 years of injection. Initially, reservoir shut-in pressure was identical in both cases but it gradually diverged as more gas was injected and the pressure difference was continuously increasing with time. The variation in reservoir storage capacity and plume migration just amongst the heterogeneous cases themselves is very small. This is because the increase in coefficient of variation for matrix porosity is small among the heterogeneous cases.
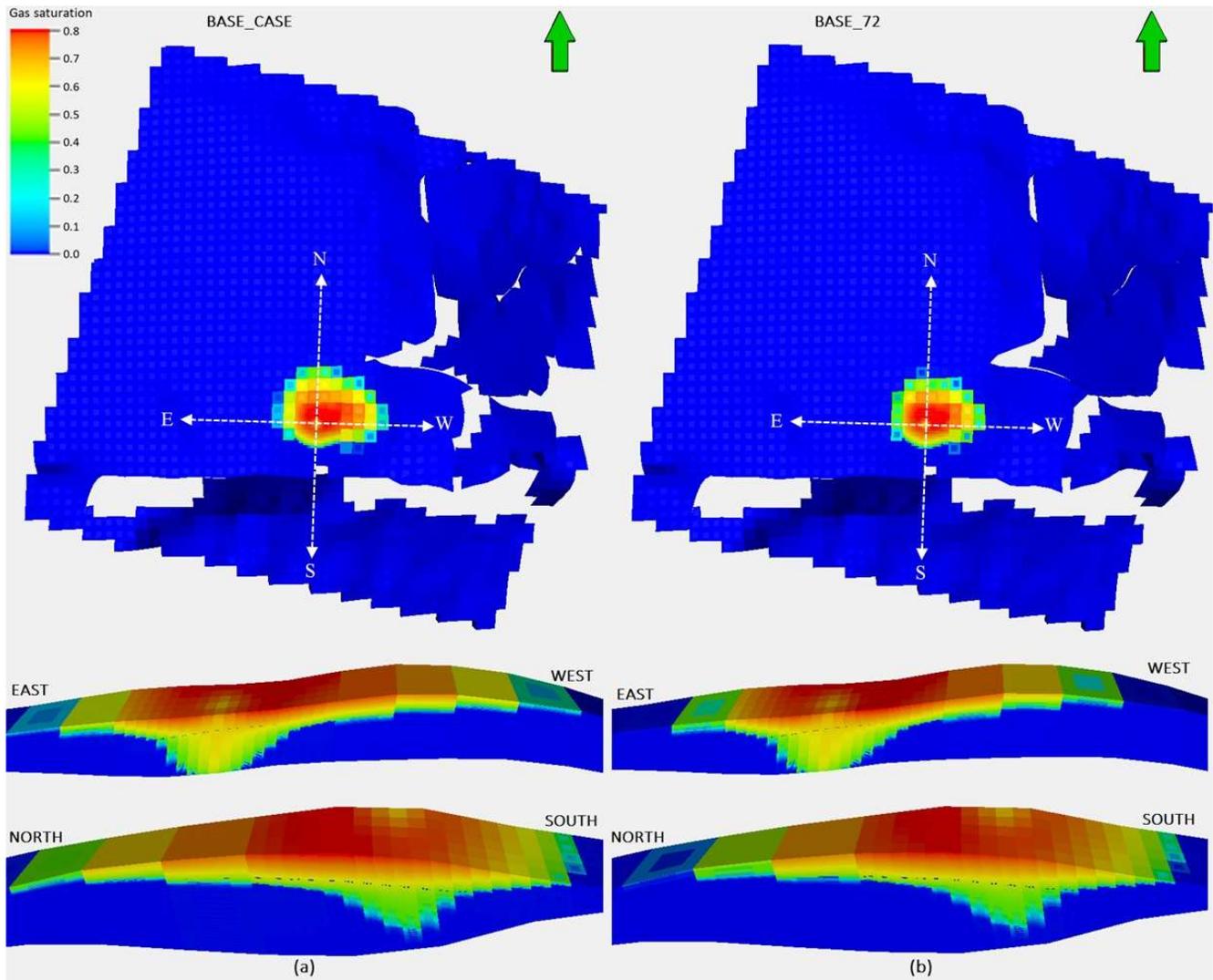
Figure 13. Part (a) shows the migration of CO_2 plume in the base case and part (b) shows migration in case base_72 over 50 years of gas injection. The same volume of CO_2 was injected but the migration of plume was different in both cases as porosity changes.
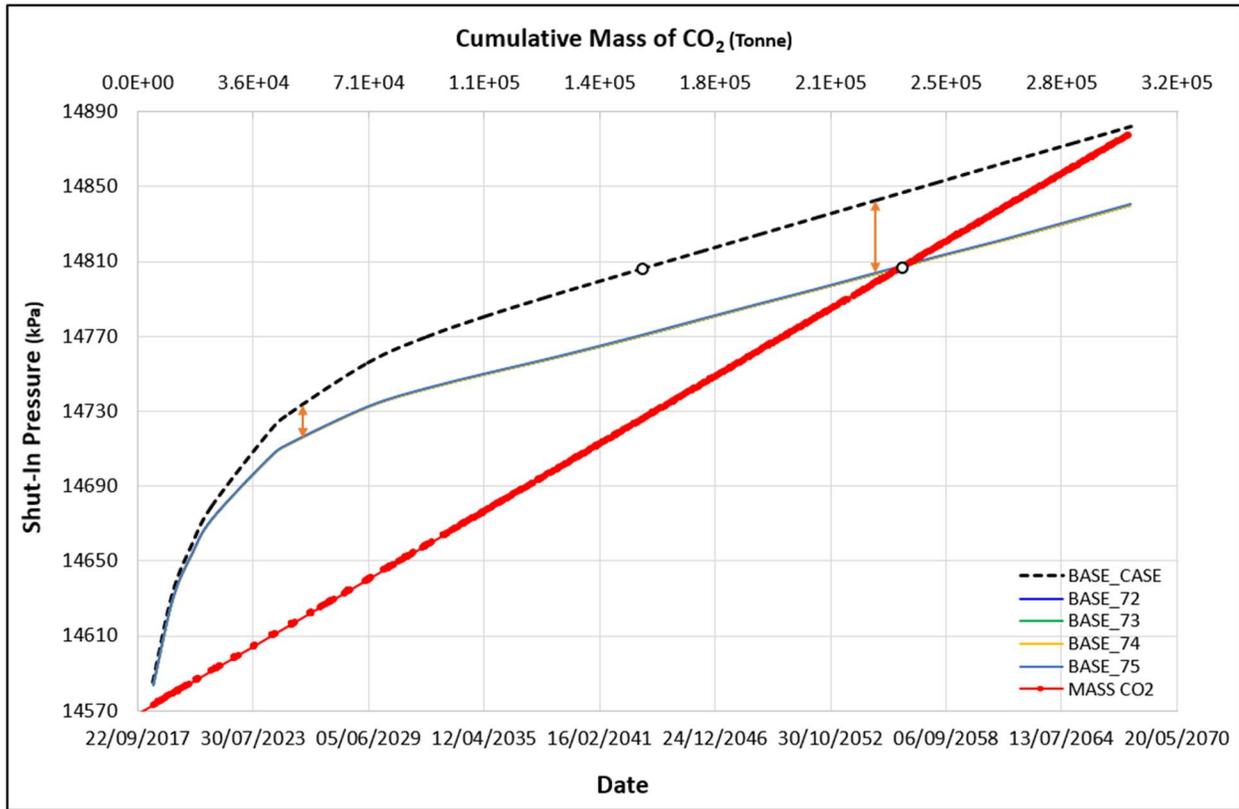
Figure 14. Reservoir shut-in pressure versus the cumulative injected mass of CO_2 for a similar time period. The heterogeneity of the simulated models based on the variation in matrix porosity.

4.2.3 Effect of kf and km

When the degree of matrix and fracture permeability variation in the horizontal direction was similar, the CO_2 plume migrated the same distance from the injection well in both cases. However, the change in gas saturation at the outer periphery of the plume was slightly different between the two cases. It was observed that the CO_2 plume migration in each of the horizontal and vertical directions was almost identical when either matrix or fracture permeability of the base case was doubled separately. The plume migration in the base case is compared in Figure 15 to cases when k_{my} and k_{fy} were each individually doubled.

The reservoir pressure response was more substantially different, compared to the changes in plume migration, when the matrix and fracture Y-direction permeabilities for the base case were doubled. The reservoir pressure depends on the ease of plume flow which seemed relatively more convenient when fracture permeability was increased compared to the matrix at the same rate in this case. It was observed that the reservoir shut-in pressure gradually increased by 16 kPa more in the case when the matrix Y-direction permeability was doubled, compared to the corresponding case of increased fracture Y-direction permeability, and stayed constant over 50 years of injection. The degree of k_{my} and k_{fy} change is identical but the shift in pressure is higher in the matrix case which verifies that the fluid prefers to flow through fractures instead of matrix. However, by doubling the matrix permeability of base case reservoir storage capacity increased 3.85 times more than the original capacity at a pressure of 14,850 kPa as can be seen in Figure 16. While the pressure of the base case decreased 68 kPa on doubling the k_m over 50 years of injection.
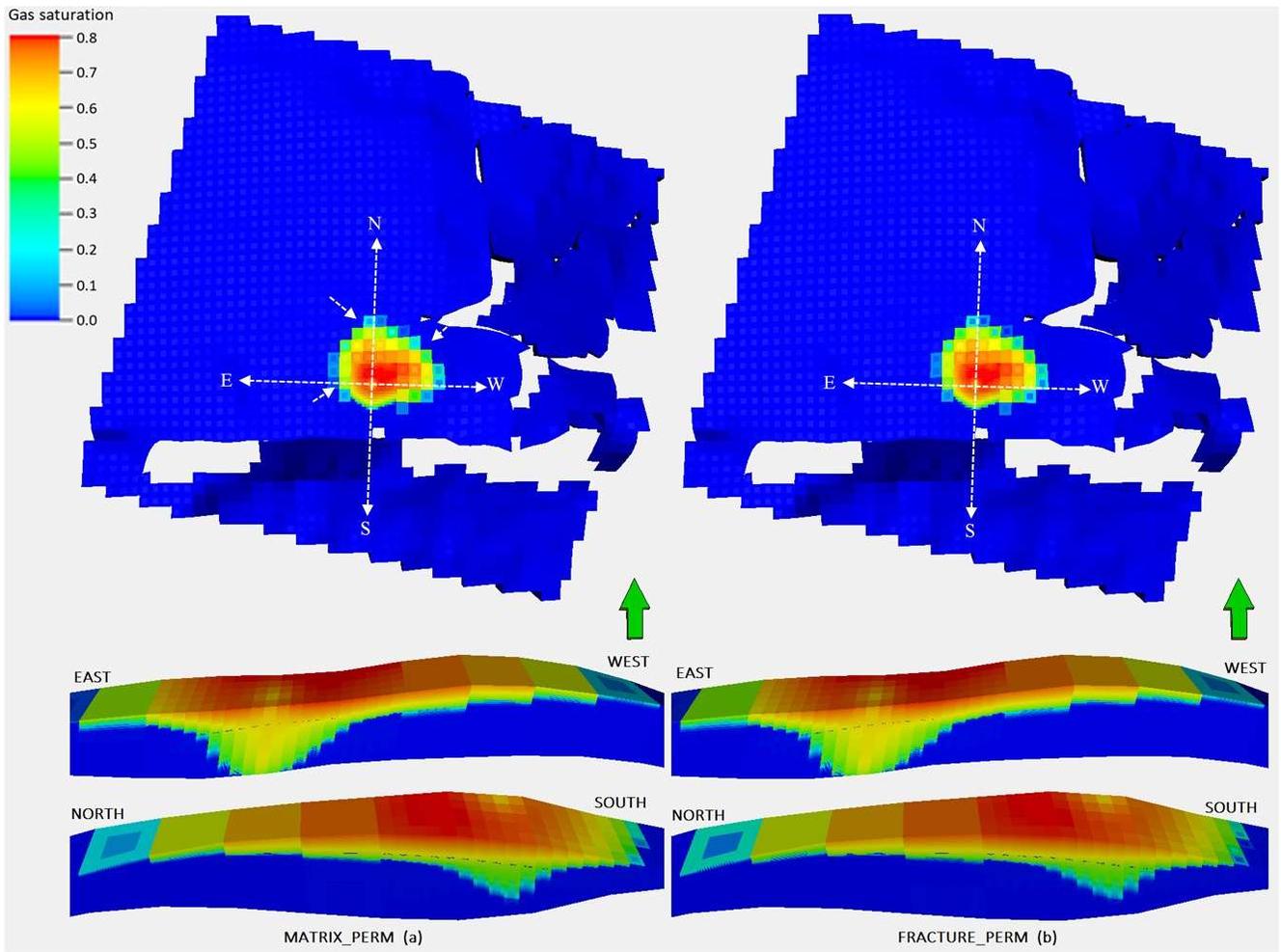
Figure 15. Comparison of CO_2 plume migration in all directions from the injection well when a change in the matrix or fracture permeability in the y-direction is twice higher compared to the base case in part (a) and (b) respectively. The CO_2 plume spread in both cases is almost identical but there is slightly higher gas saturation in the matrix case at the outer periphery of the plume and pointed out with the arrows.
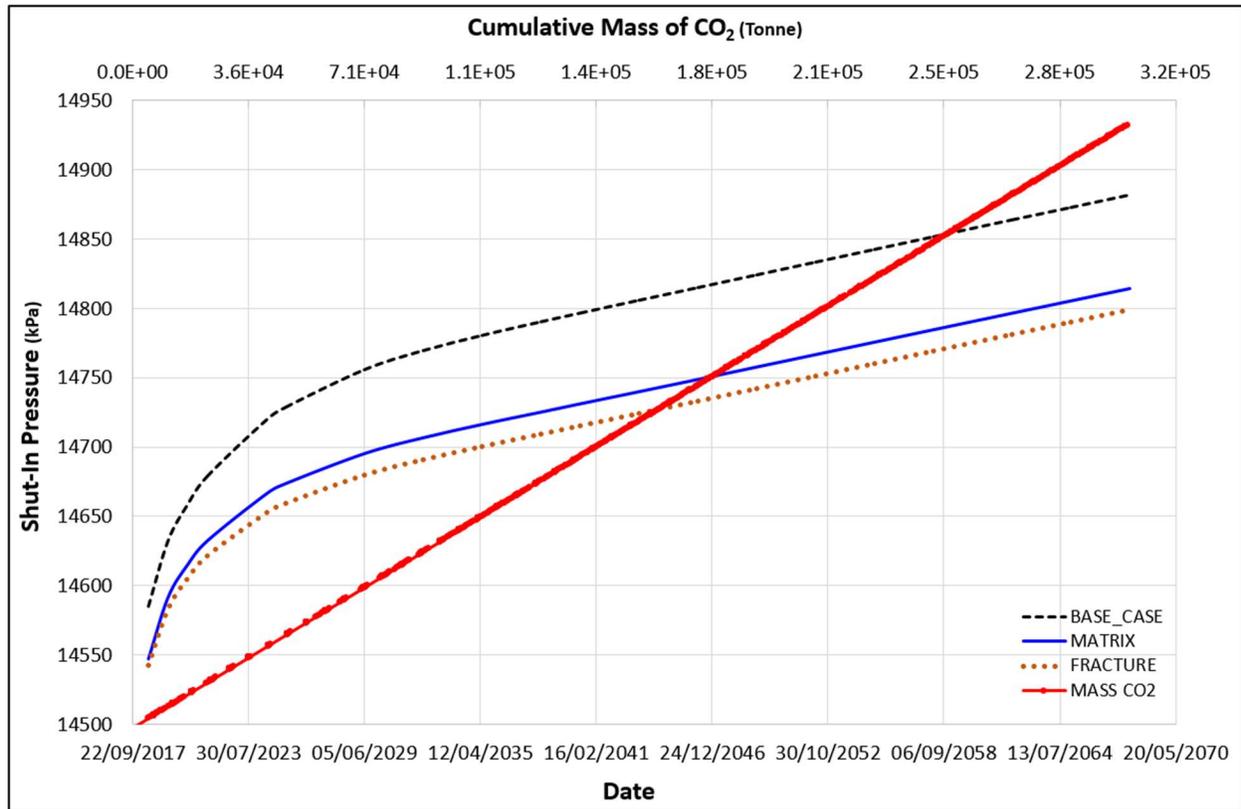
Figure 16. Comparison of reservoir shut-in pressures over 50 years of gas injection for the base case when increasing either matrix or fracture permeability in the Y-direction by a factor of two. The red dotted line shows the cumulative mass injection of CO_2 for fifty years.

4.2.4   Effect of k_v/k_h Ratio

An increase in the matrix k_v/k_h ratio increased the rate of vertical movement of gas during the injection phase. There might be a risk of gas leakage through the aquifer boundaries if k_v/k_h ratio is decreased because the horizontal migration of CO_2 may dominate in that condition. Figure 17 shows the horizontal and vertical migration of the CO_2 plume in the base case when vertical to horizontal permeability ratios were decreased from 1 to 0.0001 for a similar period of time at the same injection rate. However, when the k_v/k_h ratio was equal to 1 the gas plume was mainly migrating towards the top of the structure and accumulating under the caprock. The reservoir shut-in pressure did not significantly change when the matrix k_v/k_h ratio varied from 0.0001 to 1. The difference in reservoir pressure between the extreme cases was less than 15 kPa after 50 years of gas injection as illustrated in Figure 18. The small pressure difference, as a result of a significant change in vertical permeability of matrix, could be attributed to flow through the fractures which counterbalanced the pressure build-up by increasing the fracture flow. The reservoir storage capacity was enhanced by 16% more when k_v/k_h was increased from 0.0001 to 1 in the base case at a pressure of 15,722 kPa. It could be speculated that an increase in kv/kh, from 0.0001 to 1, comparatively enhanced the mobility of the CO_2 plume in both the horizontal and vertical directions, which improved the pore fluid and rock surface exposure to CO_2. There was no influence of faults transmissibility on CO_2 migration in this case.
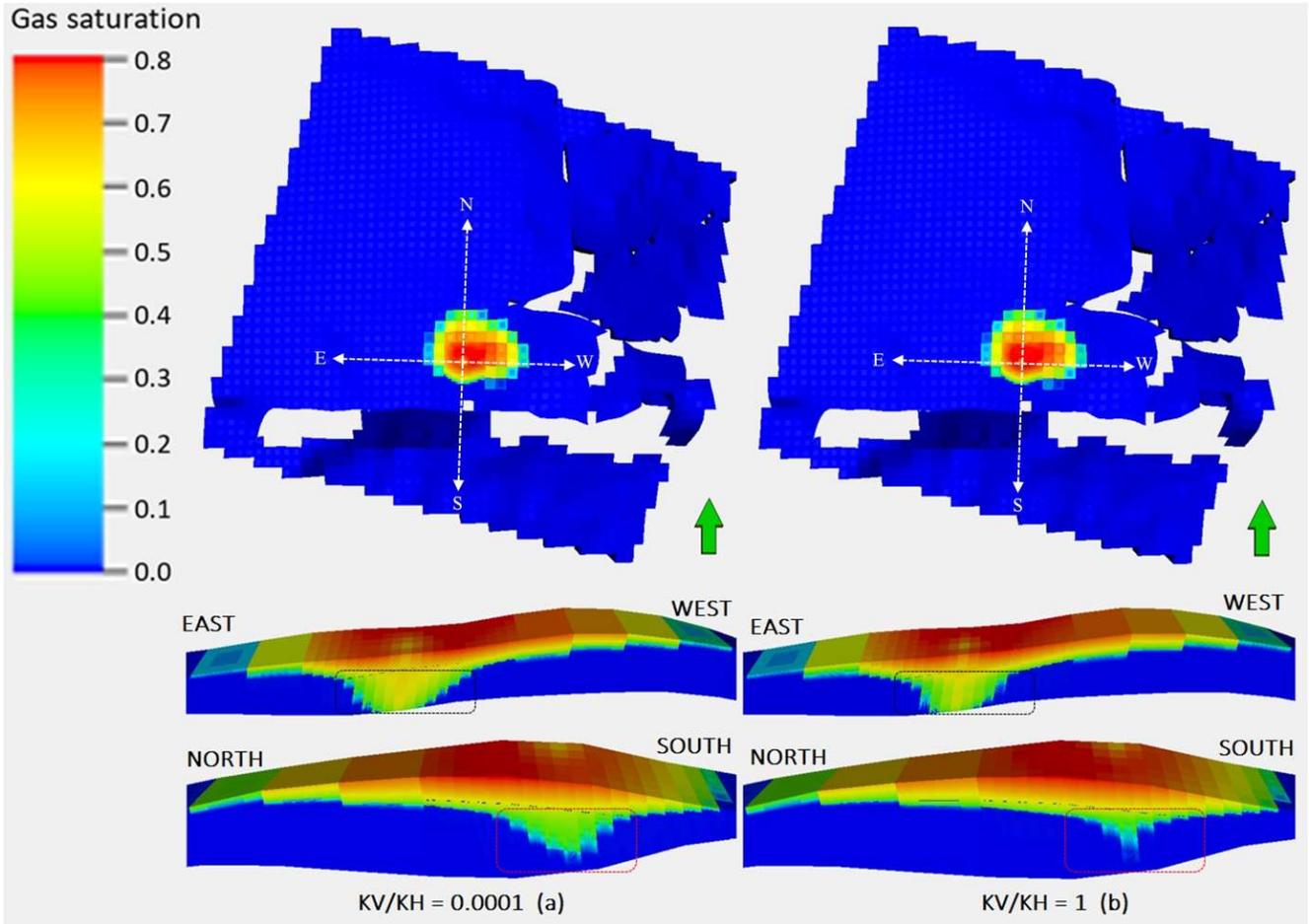
Figure 17. Movement of CO_2 plume in the horizontal and vertical direction when k_v/k_h increased from 0.0001 to 1 (a) and (b) respectively during gas injection for 50 years in the base case. The E-W & N-S segments of the reservoir are taken from the part in which the injection well is located. The black rectangles shown are to highlight the key differences between cases.
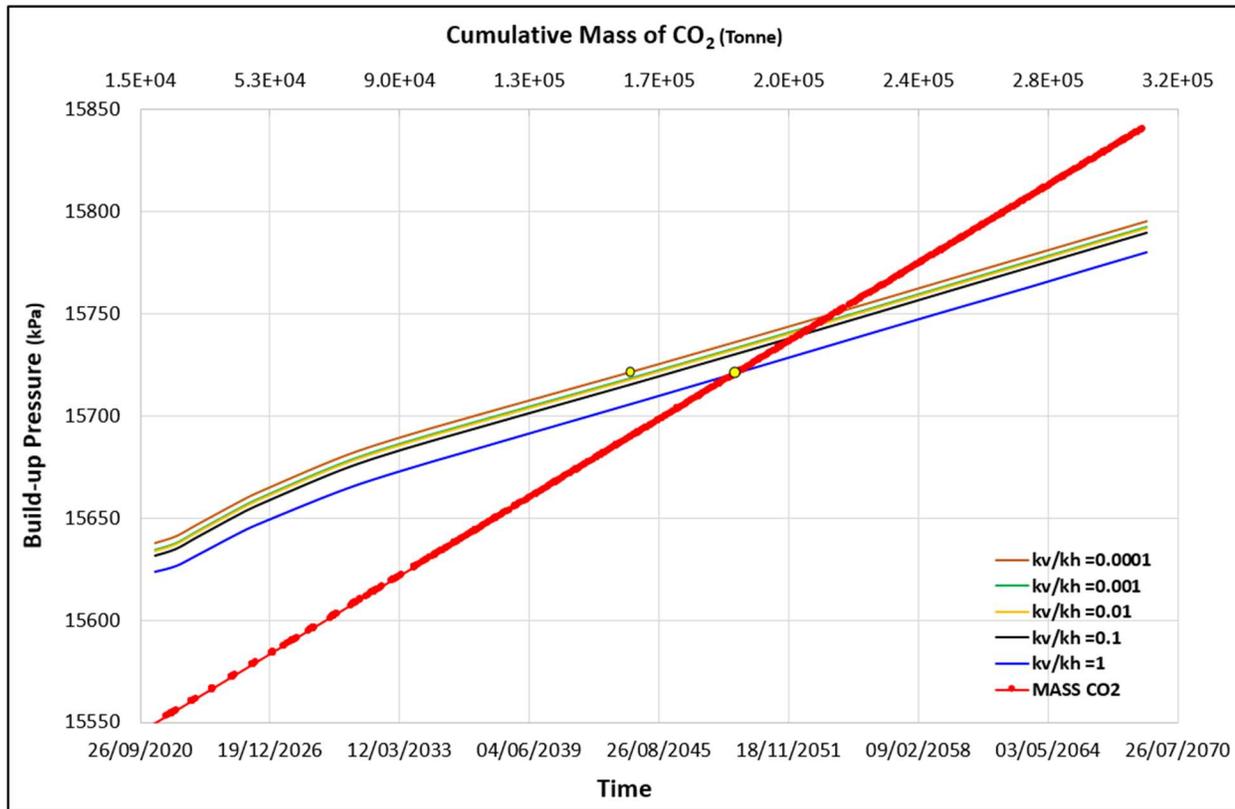
Figure 18. Simulated pressure build-up over 50 years of gas injection when k_v/k_h of the matrix was gradually decreased from 1 to 0.0001 for the base case. The plot shows pressure build-up and cumulative mass injection during the prediction phase.

4.2.5 Effect of Faults Transmissibility

There are eight faults inferred at the top of the reservoir from the 3-D seismic interpretations and are assumed to be vertical within the reservoir. Two main faults cross the storage complex from the reservoir to the overburden, which limits the south-eastward extension of the reservoir. These faults are the F11 (Ubierna fault), located at the southern part, and the F9 (East fault) located at the eastern part of the Hontomín site. The location of all the eight faults, and the migration distance of the CO_2 plume from the injection well (HI_G) following 200 years of gas injection in a fully non-sealing scenario of the base case, are shown in Figure 19.

The transmissibilities of all the faults were varied from 0 (complete barrier) to 1 (fully transmissive) in a sensitivity study. The fault transmissibility multiplier values together with the simulation cases that were used in the sensitivity study are given in Table 6. After 200 years of simulated time, the CO_2 plume could still not reach the boundaries of the reservoir at the injection rate which was used in the historical data. The gas and water injection rates in the predictive simulation study followed the in-situ injection strategy as used in the historical data. The influence of the transmissibility of most of the faults on the migration of the CO_2 plume was not apparent over 200 years of gas injection. Only the influence of the F11 and R4+5 faults was observed, which were the faults located within the range of CO_2 plume spread. The influence of the transmissibility of fault F11 (Ubierna fault) on the migration of the CO_2 plume was greater than for the fault R4+5 in the given scenario. It was observed that the shut-in reservoir pressure gradually decreased when the Ubierna fault was fully transmissive, compared to the sealing state, and the pressure difference was increasing as long as gas was being injected. In contrast, the reservoir shut-in pressure slightly decreased when fault R4+5 was made fully transmissive relative to the sealing conditions.

The influence of both faults on the pressures can be seen in Figure 20 when both faults are fully transmissive, as compared to a completely sealing state. Reservoir shut-in pressured increased from 14,585 kPa to 15,482 kPa in 200 years of gas injection at the historic injection rate when all the faults were completely sealing faults. The reservoir storage capacity slightly increased under fully transmissive conditions. Therefore, the influence of fault transmissibility on reservoir storage capacity was minor like pressure.

Table 6. Faults names as defined in the Geological model and transmissibility multiplier in respective simulated cases in the sensitivity study.

Cases	TM_F11	TM_F9	TM_FJ1	TM_FJ2	TM_FJ3	TM_R3	TM_R6	TM_R4+5
Base_62	0	0	0	0	0	0	0	0
Base_63	1	0	0	0	0	0	0	0
Base_64	0	1	0	0	0	0	0	0
Base_65	0	0	1	0	0	0	0	0
Base_66	0	0	0	1	0	0	0	0
Base_67	0	0	0	0	1	0	0	0
Base_68	0	0	0	0	0	1	0	0
Base_69	0	0	0	0	0	0	1	0
Base_70	0	0	0	0	0	0	0	1
Base_71	1	1	1	1	1	1	1	1
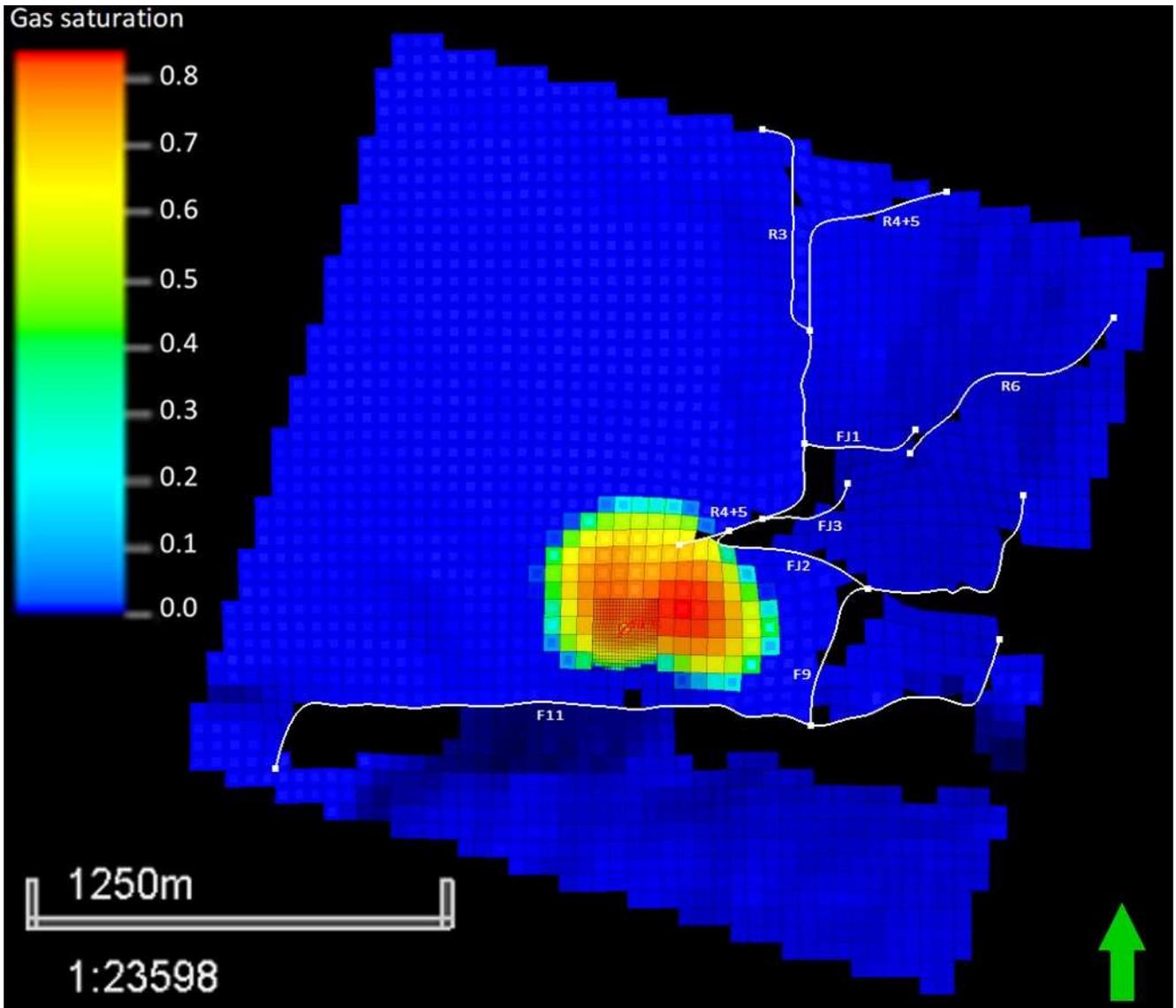
Figure 19. Location of faults in Sopeña Formation and migration distance of CO_2 plume from the injection well in 200 years of gas injection in a non-sealing scenario.
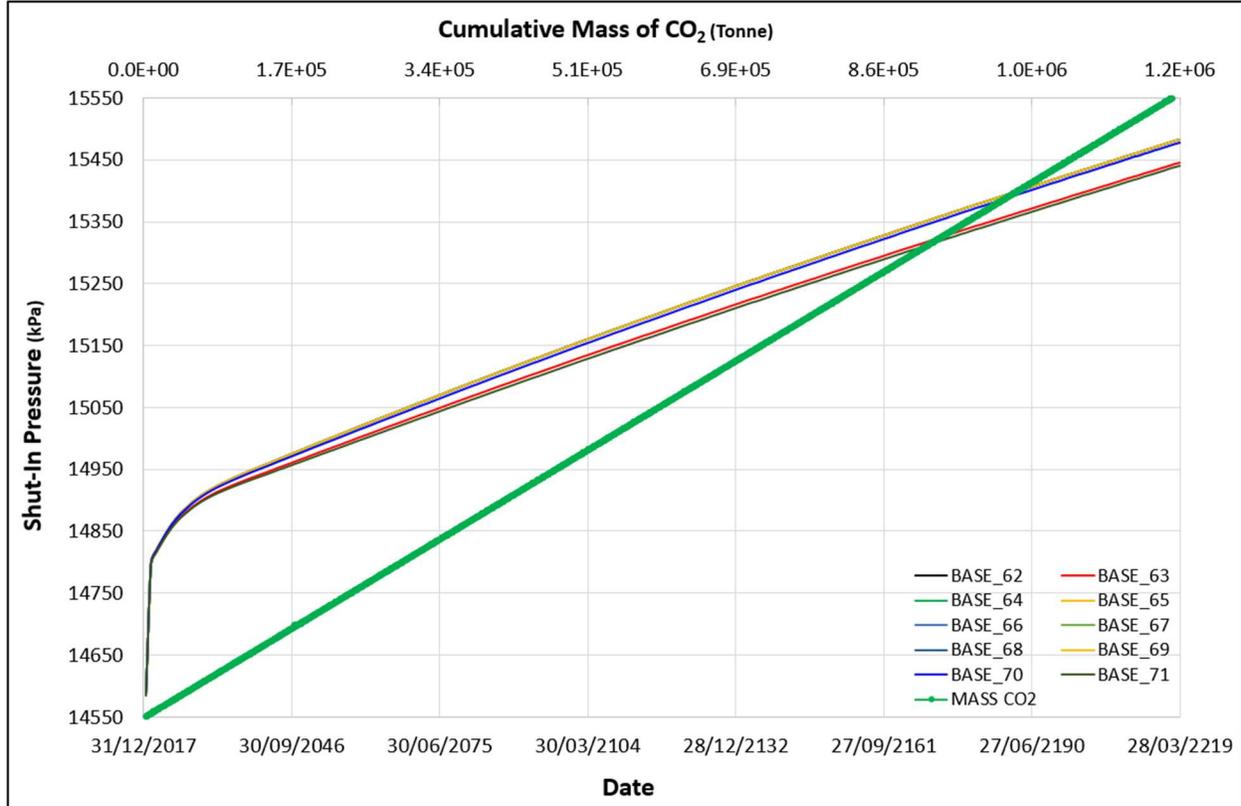
Figure 20. Influence of transmissibility of faults F11 and R4+5 on reservoir and injection pressure compared to the fully sealing case over 200 years of gas injection. The cases denoted base_63 and base_70 represent when either the fault F11 or fault R4+5, respectively, were fully transmissive as compared to base_62 which corresponds to a fully sealing state for both faults.

5 Conclusion

In this work simulations of long-term CO_2 storage in the Hontomín deep saline aquifer have been presented, with emphasis on heterogeneity effects on reservoir storage capacity, and plume migration. The fractured carbonate reservoir was simulated using the dual permeability option in E300 and validated with well test data in order to investigate the impact of heterogeneities in porosity and permeability, permeability ratio, and fault transmissibility on long term CO_2 injection. The CV parameter characterizing matrix heterogeneity was gradually increased to greater than one (CV > 1) and the impact of matrix heterogeneity variation was more prominent on reservoir storage capacity compared to the plume migration in a fractured system.

The reservoir shut-in and injection pressures gradually increased with the level of heterogeneity based on matrix permeability, but reservoir storage capacity significantly decreased. It was concluded that the fracture flow counterbalanced the matrix flow as the matrix heterogeneity increased. However, fractures do not contribute to storage therefore reservoir storage capacity drastically decreased as heterogeneity based on matrix permeability increased. It was also observed that the vertical gas migration in a homogeneous case was relatively larger compared to the heterogeneous cases and gas accumulated underneath the caprock in the process of hydrodynamic

trapping. In heterogeneous cases, gas saturation in rock layers from top to bottom is relatively high compared to the homogeneous base case for which most of the gas is stored in the topmost layer.

Plume migration, or spread, from the injection well was almost identical in both cases when either matrix or fracture permeabilities were individually multiplied by the same factor, but gas saturation in the plume was different between the two cases. The reservoir pressure increased a bit more when matrix permeability was changed by the same factor as for fractures.

The heterogeneity based on porosity variation significantly increased the reservoir storage capacity as expected and decreased the shut-in pressure compared to the homogeneous base case. The CO_2 plume spread also reduced on increasing the matrix porosity heterogeneity.

When k_v/k_h ratio was equal to 1 the gas plume mainly migrated towards the top of the structure and accumulated under the caprock. However, reservoir shut-in pressure did not significantly change when the matrix k_v/k_h ratio varied from 0.0001 to 1. This minor pressure difference as a result of a significant change in matrix permeability ratio was associated with fracture flow which counterbalanced the reduced matrix flow in a vertical direction.

The effect of faults F11 (Ubierna fault) and R4+5 on the migration of CO_2 plume and reservoir pressure were observed, out of eight normal faults, which were located in the range of CO_2 plume spread. The reservoir pressure increased by 42 kPa more when all the reservoir faults were sealing, compared to the fully transmissive scenario, over 200 years of gas injection. The influence of the faults on reservoir storage capacity was thus only minor.

Nomenclature

B_w	Water formation volume factor (bbl/STB)
CV	Coefficient of variation
C_w	Water isothermal compressibility (bar^{-1})
CO_2	Carbon dioxide
μ_w	Water viscosity (cP)
K_h	Horizontal permeability
K_v	Vertical permeability
K_f	Fracture permeability
K_{fx}	Fracture permeability in x-direction
K_{fy}	Fracture permeability in y-direction
K_{fz}	Fracture permeability in z-direction
K_m	Matrix permeability
K_{mx}	Matrix permeability in X-direction
K_{my}	Matrix permeability in Y-direction
K_{mz}	Matrix permeability in Z-direction
kPa	Kilo Pascal
K_v/k_h	Vertical to horizontal matrix permeability ratio
ϕ_f	Fracture porosity
ϕ_m	Matrix porosity
LGR	Local grid refinement
TM	Transmissibility

Acknowledgement

References

1. Al-Khdheeawi, E.A., et al., *Influence of injection well configuration and rock wettability on CO2 plume behaviour and CO2 trapping capacity in heterogeneous reservoirs.* Journal of Natural Gas Science and Engineering, 2017. **43**: p. 190-206.
2. Dai, Z., et al., *Pre-site characterization risk analysis for commercial-scale carbon sequestration.* Environ Sci Technol, 2014. **48**(7): p. 3908-15.
3. Flett, M., R. Gurton, and G. Weir, *Heterogeneous saline formations for carbon dioxide disposal: Impact of varying heterogeneity on containment and trapping.* Journal of Petroleum Science and Engineering, 2007. **57**(1-2): p. 106-118.
4. Hassanzadeh, H., M. Pooladi-Darvish, and D.W. Keith, *Accelerating CO2 Dissolution in Saline Aquifers for Geological Storage - Mechanistic and Sensitivity Studies.* Energy & Fuels, 2009. **23**(5-6): p. 3328-3336.
5. Bachu, S., W. Gunter, and E. Perkins, *Aquifer disposal of CO2: hydrodynamic and mineral trapping.* Energy Conversion and management, 1994. **35**(4): p. 269-279.
6. Doughty, C., *Investigation of CO2 Plume Behavior for a Large-Scale Pilot Test of Geologic Carbon Storage in a Saline Formation.* Transport in Porous Media, 2010. **82**(1): p. 49-76.
7. Gaus, I., *Role and impact of CO2-rock interactions during CO2 storage in sedimentary rocks.* International Journal of Greenhouse Gas Control, 2010. **4**(1): p. 73-89.
8. Gershenzon, N.I., et al., *Influence of small-scale fluvial architecture on CO2 trapping processes in deep brine reservoirs.* Water Resources Research, 2015. **51**(10): p. 8240-8256.
9. Hesse, M.A., F.M. Orr, and H.A. Tchelepi, *Gravity currents with residual trapping.* Journal of Fluid Mechanics, 2008. **611**: p. 35-60.
10. Iglauer, S., et al., *CO2 wettability of caprocks: Implications for structural storage capacity and containment security.* Geophysical Research Letters, 2015. **42**(21): p. 9279-9284.
11. Iglauer, S., et al., *Residual CO2 imaged with X-ray micro-tomography.* Geophysical Research Letters, 2011. **38**.
12. Kumar, A., et al., *Reservoir simulation of CO2 storage in deep saline aquifers.* Spe Journal, 2005. **10**(3): p. 336-348.
13. Lindeberg, E. and D. WesselBerg, *Vertical convection in an aquifer column under a gas cap of CO2.* Energy Conversion and Management, 1997. **38**: p. S229-S234.
14. Metz, B., et al., *Special Report on Carbon Dioxide Capture and Storage Prepared by the Working Group III of the Intergovernmental Panel on Climate Change.* 2005, Cambridge University Press, Cambridge.
15. Naylor, M., M. Wilkinson, and R. Haszeldine, *Calculation of CO2 column heights in depleted gas fields from known pre-production gas column heights.* Marine and Petroleum Geology, 2011. **28**(5): p. 1083-1093.
16. Pentland, C.H., et al., *Measurements of the capillary trapping of super-critical carbon dioxide in Berea sandstone.* Geophysical Research Letters, 2011. **38**.
17. Spycher, N., K. Pruess, and J. Ennis-King, *CO2-H2O mixtures in the geological sequestration of CO2. I. Assessment and calculation of mutual solubilities from 12 to 100 degrees C and up to 600 bar.* Geochimica Et Cosmochimica Acta, 2003. **67**(16): p. 3015-3031.
18. Xu, T.F., J.A. Apps, and K. Pruess, *Numerical simulation of CO2 disposal by mineral trapping in deep aquifers.* Applied Geochemistry, 2004. **19**(6): p. 917-936.

19. Lackner, K.S., *Climate change. A guide to CO2 sequestration.* Science, 2003. **300**(5626): p. 1677-8.

20. Ghanbari, S., et al., *Simulation of CO2 storage in saline aquifers.* Chemical Engineering Research & Design, 2006. **84**(A9): p. 764-775.

21. Davies, C., *European Parliament Resolution. Implementation report 2013: developing and applying carbon capture and storage technology in Europe (2013/2079(INI)).* 2013.

22. Alcalde, J., et al., *3D geological characterization of the Hontomín CO2 storage site, Spain: Multidisciplinary approach from seismic, well-log and regional data.* Tectonophysics, 2014. **627**: p. 6-25.

23. Le Gallo, Y. and J. de Dios, *Geological Model of a Storage Complex for a CO2 Storage Operation in a Naturally-Fractured Carbonate Formation.* Geosciences, 2018. **8**(9): p. 354.

24. de Dios, J.C., et al., *Hydraulic characterization of fractured carbonates for CO2 geological storage: Experiences and lessons learned in Hontomín Technology Development Plant.* International Journal of Greenhouse Gas Control, 2017. **58**: p. 185-200.

25. Lemonnier, P. and B. Bourbiaux, *Simulation of naturally fractured reservoirs. state of the art-part 1– physical mechanisms and simulator formulation.* Oil & Gas Science and Technology–Revue de l'Institut Français du Pétrole, 2010. **65**(2): p. 239-262.

26. Lemonnier, P. and B. Bourbiaux, *Simulation of naturally fractured reservoirs. state of the art-Part 2– matrix-fracture transfers and typical features of numerical studies.* Oil & Gas Science and Technology– Revue de l'Institut Français du Pétrole, 2010. **65**(2): p. 263-286.

27. Egya, D.O., et al., *Analysing the limitations of the dual-porosity response during well tests in naturally fractured reservoirs.* Petroleum Geoscience, 2019. **25**(1): p. 30-49.

28. Bennion, B. and S. Bachu, *Drainage and imbibition relative permeability relationships for supercritical CO2/brine and H2S/brine systems in intergranular sandstone, carbonate, shale, and anhydrite rocks.* SPE Reservoir Evaluation & Engineering, 2008. **11**(03): p. 487-496.

29. Dandekar, A.Y., *Petroleum reservoir rock and fluid properties.* 2013: CRC press.

30. Skjaeveland, S.M., et al., *Capillary pressure correlation for mixed-wet reservoirs.* Spe Reservoir Evaluation & Engineering, 2000. **3**(1): p. 60-67.

31. Spycher, N. and K. Pruess, *A Phase-Partitioning Model for CO2-Brine Mixtures at Elevated Temperatures and Pressures: Application to CO2-Enhanced Geothermal Systems.* Transport in Porous Media, 2010. **82**(1): p. 173-196.

32. Fenghour, A., W.A. Wakeham, and V. Vesovic, *The viscosity of carbon dioxide.* Journal of Physical and Chemical Reference Data, 1998. **27**(1): p. 31-44.

33. Cooper, J. and R. Dooley, *The International Association for the Properties of Water and Steam.* Release on the IAPWS formulation for the thermodynamic properties of seawater, 2008. **19**.

34. Sharqawy, M.H., J.H. Lienhard, and S.M. Zubair, *Thermophysical properties of seawater: a review of existing correlations and data.* Desalination and water treatment, 2010. **16**(1-3): p. 354-380.

35. Warren, J. and P. Root, *The Behavior of Naturally Fractured Reservoirs. SPEJ 3 (3): 245–255.* Trans., AIME, 1963. **228**.

36. Nelson, R., *Geologic analysis of naturally fractured reservoirs. Elsevier, 2001.* Elsevier, 2001.

37. Ahmed, T., *Reservoir engineering handbook.* 2018: Gulf professional publishing.

38. Journel, A.G. and C.J. Huijbregts, *Mining geostatistics.* Vol. 600. 1978: Academic press London.

39. Rashid, F., et al., *Porosity and permeability of tight carbonate reservoir rocks in the north of Iraq.* Journal of Petroleum Science and Engineering, 2015. **133**: p. 147-161.

40.   He, L., et al., *Complex relationship between porosity and permeability of carbonate reservoirs and its controlling factors: A case study of platform facies in Pre-Caspian Basin.* Petroleum Exploration and Development, 2014. **41**(2): p. 225-234.

41.   Chen, C., L. Zeng, and L. Shi, *Continuum-scale convective mixing in geological CO2 sequestration in anisotropic and heterogeneous saline aquifers.* Advances in water resources, 2013. **53**: p. 175-187.

42.   Rapaka, S., et al., *Non-modal growth of perturbations in density-driven convection in porous media.* Journal of Fluid Mechanics, 2008. **609**: p. 285.

43.   Xu, X., S. Chen, and D. Zhang, *Convective stability analysis of the long-term storage of carbon dioxide in deep saline aquifers.* Advances in water resources, 2006. **29**(3): p. 397-407.

44.   Farajzadeh, R., et al., *The effect of heterogeneity on the character of density-driven natural convection of CO2 overlying a brine layer.* Advances in Water Resources, 2011. **34**(3): p. 327-339.

45.   Lengler, U., M. De Lucia, and M. Kühn, *The impact of heterogeneity on the distribution of CO2: Numerical simulation of CO2 storage at Ketzin.* International Journal of Greenhouse Gas Control, 2010. **4**(6): p. 1016-1025.

46.   Tian, H., et al., *Impacts of hydrological heterogeneities on caprock mineral alteration and containment of CO2 in geological storage sites.* International Journal of Greenhouse Gas Control, 2014. **24**: p. 30-42.

47.   Hu, B.X., et al., *Examining the influence of heterogeneous porosity fields on conservative solute transport.* Journal of Contaminant Hydrology, 2009. **108**(3-4): p. 77-88.

48.   Pan, F., et al., *Incorporating layer-and local-scale heterogeneities in numerical simulation of unsaturated flow and tracer transport.* Journal of contaminant hydrology, 2009. **103**(3-4): p. 194-205.

49.   Pan, F., et al., *Sensitivity analysis of unsaturated flow and contaminant transport with correlated parameters.* Journal of hydrology, 2011. **397**(3-4): p. 238-249.